Cell Reports

Article

Host-Derived Lipids from Tuberculous Pleurisy Impair Macrophage Microbicidal-Associated Metabolic Activity

Graphical Abstract

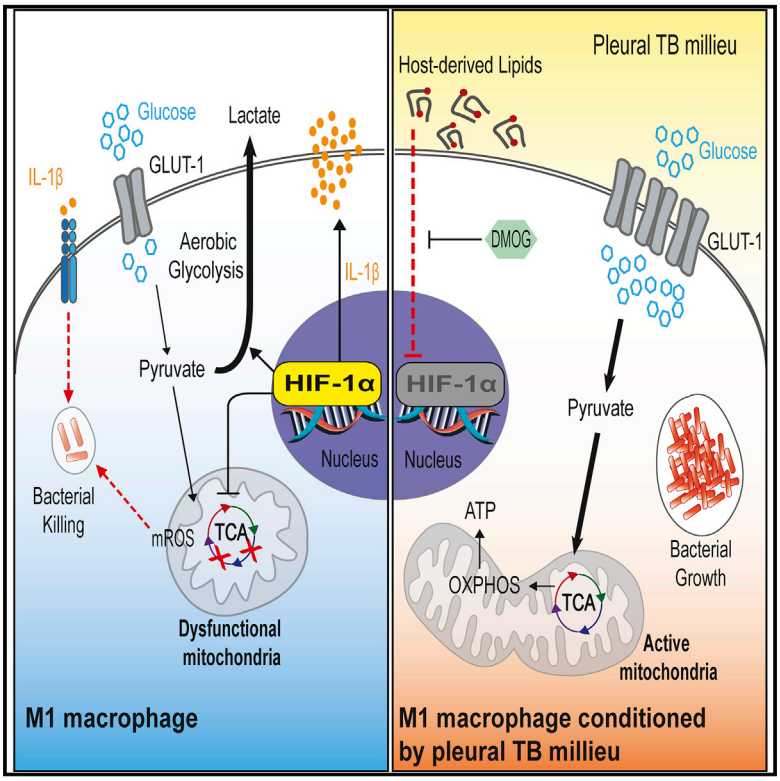

Highlights

- Tuberculous pleural effusion (TB-PE) shifts glycolysis to OXPHOS in M1 macrophages
- Metabolic shift is accompanied by low HIF-1α activity and high *M. tuberculosis* burden
- HIF-1α stabilization reverts the metabolic shift and inhibitory effects of TB-PE
- Host-derived lipids (eicosanoid-enriched fraction) in TB-PE drive the metabolic shift

Authors

José Luis Marín Franco, Melanie Genoula, Dan Corral, ..., María Del Carmen Sasiain, Geanncarlo Lugo-Villarino, Luciana Balboa

Correspondence

lugo@ipbs.fr (G.L.-V.), luciana_balboa@hotmail.com (L.B.)

In Brief

The metabolic state is a clear yet confounding factor in macrophages to control *M. tuberculosis*. In this issue, Marín Franco et al. reveal that a tuberculosis-associated microenvironment triggers the shift from aerobic glycolysis to OXPHOS by inhibiting HIF-1α activity, rendering M1 macrophages susceptible to *M. tuberculosis* infection. Host-derived lipids in this microenvironment are responsible for the metabolic shift and inhibitory effects on pro-inflammatory and microbicidal macrophage properties.

Marín Franco et al., 2020, Cell Reports *33*, 108547
December 29, 2020
https://doi.org/10.1016/j.celrep.2020.108547

CellPress

Cell Reports

CellPress
OPEN ACCESS

Article

Host-Derived Lipids from Tuberculous Pleurisy Impair Macrophage Microbicidal-Associated Metabolic Activity

José Luis Marín Franco,[1,2] Melanie Genoula,[1,2,11] Dan Corral,[3,11] Gabriel Duette,[4] Malena Ferreyra,[1,2] Mariano Maio,[1] María Belén Dolotowicz,[1] Omar Emiliano Aparicio-Trejo,[5] Eduardo Patiño-Martínez,[6] Alison Charton,[3] Arnaud Métais,[3] Federico Fuentes,[1] Vanessa Soldan,[7] Eduardo José Moraña,[8] Domingo Palmero,[8] Matías Ostrowski,[4] Pablo Schierloh,[2,9] Carmen Sánchez-Torres,[6] Rogelio Hernández-Pando,[10] José Pedraza-Chaverri,[5] Yoann Rombouts,[3] Denis Hudrisier,[3] Emilie Layre,[3] Christel Vérollet,[2,3] Isabelle Maridonneau-Parini,[2,3] Olivier Neyrolles,[2,3] María Del Carmen Sasiain,[1,2] Geanncarlo Lugo-Villarino,[2,3,12,13,14,*] and Luciana Balboa[1,2,12,13,*]

[1]Instituto de Medicina Experimental (IMEX)-CONICET, Academia Nacional de Medicina, Buenos Aires C1425ASU, Argentina
[2]International Associated Laboratory (LIA) CNRS IM-TB/HIV (1167), Buenos Aires, Argentina - Toulouse, France
[3]Institut de Pharmacologie et de Biologie Structurale, Université de Toulouse, CNRS, UPS, Toulouse 31077, France
[4]Instituto de Investigaciones Biomédicas en Retrovirus y SIDA (INBIRS), Facultad de Medicina, Universidad de Buenos Aires, Buenos Aires C1121ABG, Argentina
[5]Department of Biology, Faculty of Chemistry, National Autonomous University of Mexico (UNAM), Mexico City 04510, Mexico
[6]Departamento de Biomedicina Molecular, CINVESTAV, Mexico City 07360, Mexico
[7]METi, Centre de Biologie Intégrative, Université de Toulouse, CNRS, UPS, Toulouse 31062, France
[8]Instituto Prof. Dr. Raúl Vaccarezza, Hospital de Infecciosas Dr. F.J. Muñiz, Buenos Aires C1282AFE, Argentina
[9]Instituto de I+D en Bioingenieria y Bioinformática (IBB)-UNER-CONICET, Entre Ríos 3100, Argentina
[10]Department of Pathology, National Institute of Medical Science and Nutrition, Salzador Zubiran, Mexico City 14080, Mexico
[11]These authors contributed equally
[12]These authors contributed equally
[13]Senior author
[14]Lead Contact
*Correspondence: lugo@ipbs.fr (G.L.-V.), luciana_balboa@hotmail.com (L.B.)
https://doi.org/10.1016/j.celrep.2020.108547

SUMMARY

Mycobacterium tuberculosis (Mtb) regulates the macrophage metabolic state to thrive in the host, yet the responsible mechanisms remain elusive. Macrophage activation toward the microbicidal (M1) program depends on the HIF-1α-mediated metabolic shift from oxidative phosphorylation (OXPHOS) toward glycolysis. Here, we ask whether a tuberculosis (TB) microenvironment changes the M1 macrophage metabolic state. We expose M1 macrophages to the acellular fraction of tuberculous pleural effusions (TB-PEs) and find lower glycolytic activity, accompanied by elevated levels of OXPHOS and bacillary load, compared to controls. The eicosanoid fraction of TB-PE drives these metabolic alterations. HIF-1α stabilization reverts the effect of TB-PE by restoring M1 metabolism. Furthermore, Mtb-infected mice with stabilized HIF-1α display lower bacillary loads and a pronounced M1-like metabolic profile in alveolar macrophages (AMs). Collectively, we demonstrate that lipids from a TB-associated microenvironment alter the M1 macrophage metabolic reprogramming by hampering HIF-1α functions, thereby impairing control of Mtb infection.

INTRODUCTION

Tuberculosis (TB) is a highly contagious disease caused by the bacterial pathogen *Mycobacterium tuberculosis* (Mtb). Although treatment of TB is now standardized, it remains one of the top 10 causes of death worldwide, with 10 million new cases and 1.2 million deaths among human immunodeficiency virus (HIV)-negative people in 2018 (World Health Organization, 2019). Chronic host-pathogen interaction in TB leads to extensive metabolic remodeling in both the host and the pathogen (Russell et al., 2009). In fact, the success of Mtb as a pathogen largely relies on its ability to adapt to the intracellular milieu of human macrophages.

Macrophages can modify their metabolic functions from a healing/growth-promoting setting (M2 macrophages) toward a killing/inhibitory capacity (M1 macrophages) (Mills, 2012; Mills et al., 2000), representing opposing ends of the full activation spectrum. M1 macrophages, generally induced by interferon-γ (IFN-γ) and/or lipopolysaccharide (LPS) stimulation, are endowed with microbicidal properties; M2 macrophages, generally induced upon interleukin-4 (IL-4) or IL-13 stimulation, are oriented toward an immunomodulatory and poorly microbicidal

phenotype, resulting in impaired anti-mycobacterial properties (Kahnert et al., 2006; Martinez et al., 2009; Raju et al., 2008). Cellular metabolism and metabolic pathways not only provide energy but also regulate macrophage phenotype and function (Van den Bossche et al., 2017), suggesting that metabolic pathways represent a target for pathogens to evade the host immune response. Particularly, M1 macrophages undergo a metabolic switch toward glycolysis and away from oxidative phosphorylation (OXPHOS) (Kelly and O'Neill, 2015). This glycolytic reprogramming is characterized by an increase in the aerobic glycolysis that results in lactate release and a decrease in the flux of tricarboxylic acid (TCA) cycle and subsequent OXPHOS (Gleeson and Sheedy, 2016; Kelly and O'Neill, 2015). Reduction of the OXPHOS pathway is associated with an increase in the production of mitochondrial reactive oxygen species (mROS) endowed with antimicrobial capacity (West et al., 2011). Metabolic reprogramming taking place in M1 macrophages is orchestrated by the hypoxia-inducible factor-1 alpha (HIF-1α), which increases the expression of glycolytic enzymes and pro-inflammatory cytokines (e.g., IL-1β) while inhibiting OXPHOS activity (Gleeson and Sheedy, 2016; Palsson-Mcdermott et al., 2015).

Within the framework of macrophage metabolism and its impact on TB, it was recently reported in the mouse model that alveolar macrophages (AMs) and interstitial macrophages (IMs) differ in their ability to control Mtb intracellular growth, which depends on the predominant metabolic status (Huang et al., 2018). A transcriptomic analysis revealed that IMs were glycolytically active, whereas AMs were committed to fatty acid oxidation and exhibited higher susceptibility to bacterial replication than IMs (Huang et al., 2018). Moreover, Mtb infection leads to glycolysis in bone-marrow-derived macrophages (Koo et al., 2012; Mehrotra et al., 2014), lungs of infected mice (Shi et al., 2015), and lung granulomas from patients with active TB (Subbian et al., 2015). Of note, Mtb infection increases HIF-1α expression in IFN-γ-activated macrophages, which is essential for the IFN-γ-dependent control of infection (Braverman et al., 2016). Despite these toxic effects enacted by direct infection of cells, Mtb still survives and manages to shift the microenvironment in its favor, which led us to hypothesize that local factors found in the lung milieu may regulate the metabolic network of macrophages and their microbicidal properties. The main goal of our study was to evaluate whether human lung milieu generated during Mtb infection interferes with the metabolic network associated with the M1 macrophage profile and modulates the immune response to favor the mycobacteria.

To address this issue, we used the tuberculous pleural effusion (TB-PE) as a physiologically relevant fluid reflecting the microenvironment found in a human respiratory cavity that is impacted by Mtb infection (Genoula et al., 2018, 2020; Lastrucci et al., 2015). The pleural effusion (PE) is an excess of fluid recovered from pleural space characterized by a high protein content and specific leukocytes (Vorster et al., 2015). Although pleural TB is generally categorized as extrapulmonary, there is an intimate anatomic relationship between the pleura and the pulmonary parenchyma (Seibert et al., 1991). Compared to blood or serum, TB-PE better reflects the microenvironment encountered in the human respiratory cavity during infection, making it a very attractive tool for TB research. Evidence for incomplete control of the infection in pleural TB comes from the fact that patients frequently develop active TB at a later time if untreated (Vorster et al., 2015), suggesting the existence of active mechanisms hampering the protective long-lasting immune response. In this regard, TB-PE shifts *ex vivo* human monocyte differentiation toward an anti-inflammatory M2-like ($CD16^+CD163^+MerTK^+p\text{-}STAT3^+$) macrophage state, reproducing the phenotype exhibited by macrophages directly isolated from the pleural cavity of TB patients and lung biopsies of non-human primates with advanced TB (Lastrucci et al., 2015). Likewise, the acellular fraction of TB-PE modifies the lipid metabolism of human macrophages, leading them into foamy macrophages and impacting their effector functions against the bacilli (Genoula et al., 2018).

In this study, we provide strong evidence that host lipids from TB-PE shifts the glycolysis-based metabolic program of M1 macrophages toward OXPHOS activity by targeting HIF-1α expression. This results in attenuation of the pro-inflammatory and microbicide properties, leading to susceptibility to Mtb intracellular growth in M1 macrophages. Pharmacological stabilization of HIF-1α expression restores not only glycolysis and pro-inflammatory properties in M1 macrophages, but also better control of the Mtb burden in human macrophages and lungs of Mtb-infected mice.

RESULTS

PE from Active TB Patients Inhibits Aerobic Glycolysis in M1 Macrophages

To evaluate whether soluble factors released during Mtb infection interfere with the metabolic network associated with the M1 profile, we generated human macrophages (M0), activated them toward the M1 profile with LPS and IFN-γ in the presence (PE-M1) or absence (M1) of the acellular fraction of TB-PEs, and evaluated metabolic parameters as well as M1 macrophage-associated cell-surface markers. TB-PE treatment did not induce cell death in our experimental conditions (Figures S1A–S1C). The M1-associated cell-surface markers HLA-DR, CD86, and PD-L1 were upregulated to a similar extent in M1 and PE-M1 macrophages in response to IFN-γ and LPS, while CD80 was upregulated to a lesser extent in PE-M1 than M1 macrophages (Figure S1D). Therefore, it appears that the TB-PE treatment does not affect the establishment of the M1 activation program in human macrophages.

Since glucose metabolism in macrophages plays a key role in mounting a robust, pro-inflammatory response to bacterial infection, we evaluated the expression of the glucose transporter GLUT1 (SLC2A1) by flow cytometry using an anti-Glut-1 antibody (Figure 1A) or the Glut-1 ligand $H2_{RBD}$-EGFP (Kinet et al., 2007) (Figure 1B). We also measured glucose incorporation through the estimation of its consumption from supernatant media (Figure 1C) and the uptake of fluorescent d-glucose analog 2-[N-(7-nitrobenz-2-oxa-1,3-diazol-4-yl) amino]-2-deoxy-D–glucose (2-NBDG) (Figure 1D). In line with the literature, M1 macrophages displayed higher levels of both GLUT1 expression and glucose uptake than M0 macrophages, and these levels further increased after TB-PE treatment (Figures 1A–1D).

Next, we wondered whether this increased glucose influx was used to fuel the glycolytic pathway leading to the production of

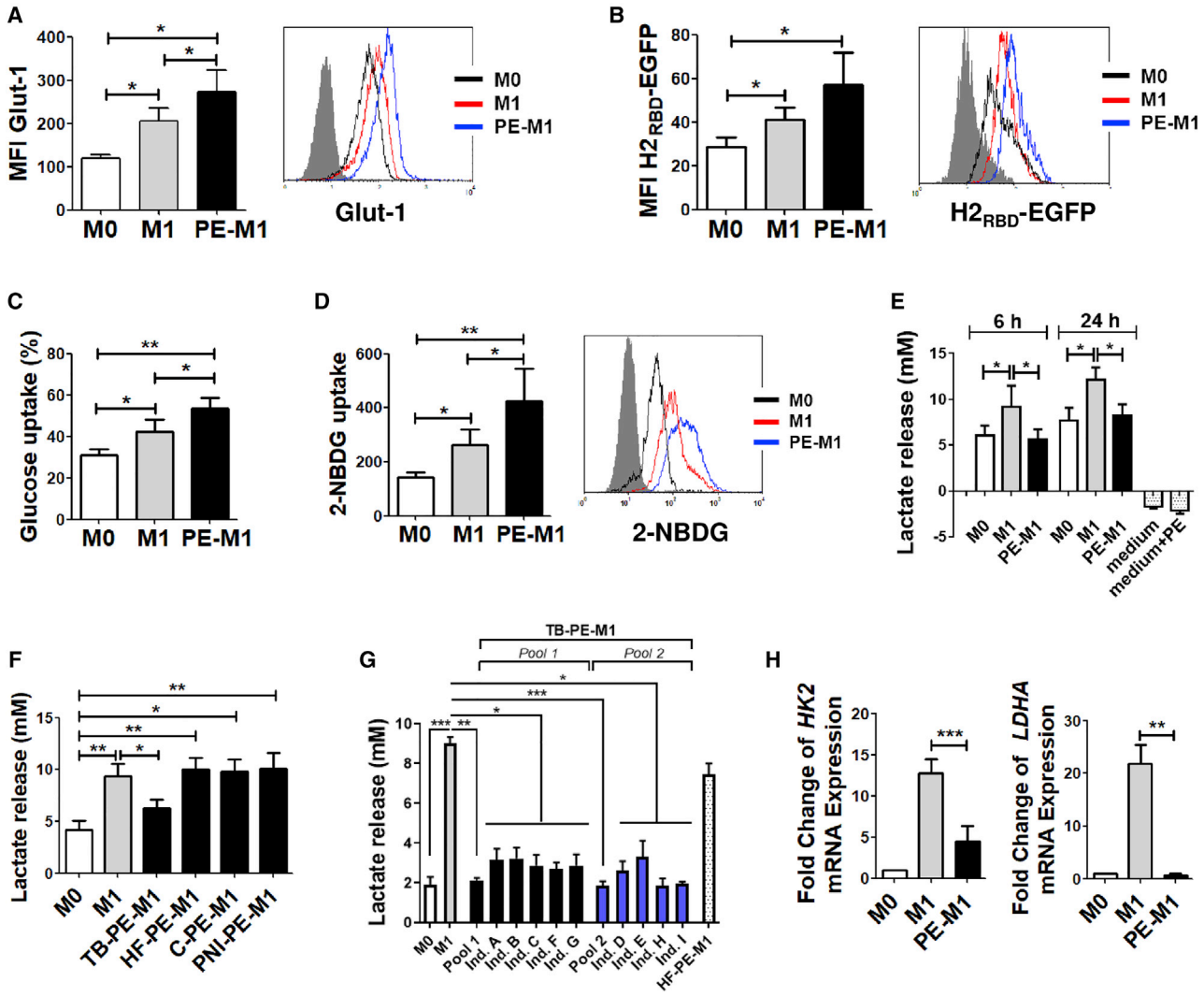

Figure 1. Pleural Effusion from Active TB Patients Inhibits Aerobic Glycolysis in M1 Macrophages

GM-CSF-driven human macrophages (M0) were polarized toward the M1 profile with LPS and IFN-γ in the presence (PE-M1) or absence (M1) of the acellular fraction of tuberculous pleural effusions (TB-PEs).

(A and B) Mean fluorescence intensity (MFI) of Glut-1 measured though the binding of the cells to the anti-Glut-1 antibody (A; n = 8) and the Glut-1 ligand $H2_{RBD}$-EGFP (B; n = 4). Representative histograms are shown.

(C) Glucose uptake measured in supernatant (n = 6).

(D) Glucose consumption measured by 2-NBDG incorporation (n = 5). A representative histogram is shown.

(E and F) Lactate release measured in supernatant. HF, heart failure; C, cancer; PNI, parapneumonic PE. n = 8.

(G) Lactate release by macrophages (M0) polarized toward the M1 profile with LPS and IFN-γ in the presence (TB-PE-M1) or absence (M1) of the acellular fraction of two different pools of TB-PEs (prepared with samples from 10 different patients each), with individual TB-PE from single patients (Ind. A to Ind. I) or a pool of pleural effusions from patients with heart failure (HF-PE-M1). n = 6.

(H) Expression of lactate dehydrogenase A (*LDHA*) mRNA and hexokinase 2 (*HK2*) mRNA relative to M0. n = 5.

(A–F) Friedman test followed by Dunn's multiple comparison test (*$p < 0.05$; **$p < 0.01$), as depicted by lines. (G) Paired t test (**$p < 0.01$; ***$p < 0.001$) for M1 versus PE-M1. Values are expressed as means ± SEM.

lactate. As previously reported (Palsson-Mcdermott et al., 2015), M1 macrophages produced more lactate than M0 cells (Figure 1E). PE-M1 macrophages did not produce significantly more lactate than M0 cells (Figure 1E), whereas those macrophages exposed to PE from other patients (i.e., with cancer, pneumonia or heart failure) or serum from TB patients did (Figures 1F and S1E). Unlike pleurisy from heart failure patients, the inhibition of lactate production by macrophages appears to be a common feature of TB pleurisy, as an additional PE pool or multiple individual PE samples reproduced this effect (Figure 1G). We also evaluated the expression of the glycolytic enzymes such as lactate dehydrogenase A (LDHA), which catalyzes the conversion of lactate to pyruvate, and hexokinase 2 (HK2), which produces glucose-6-phosphate and is the

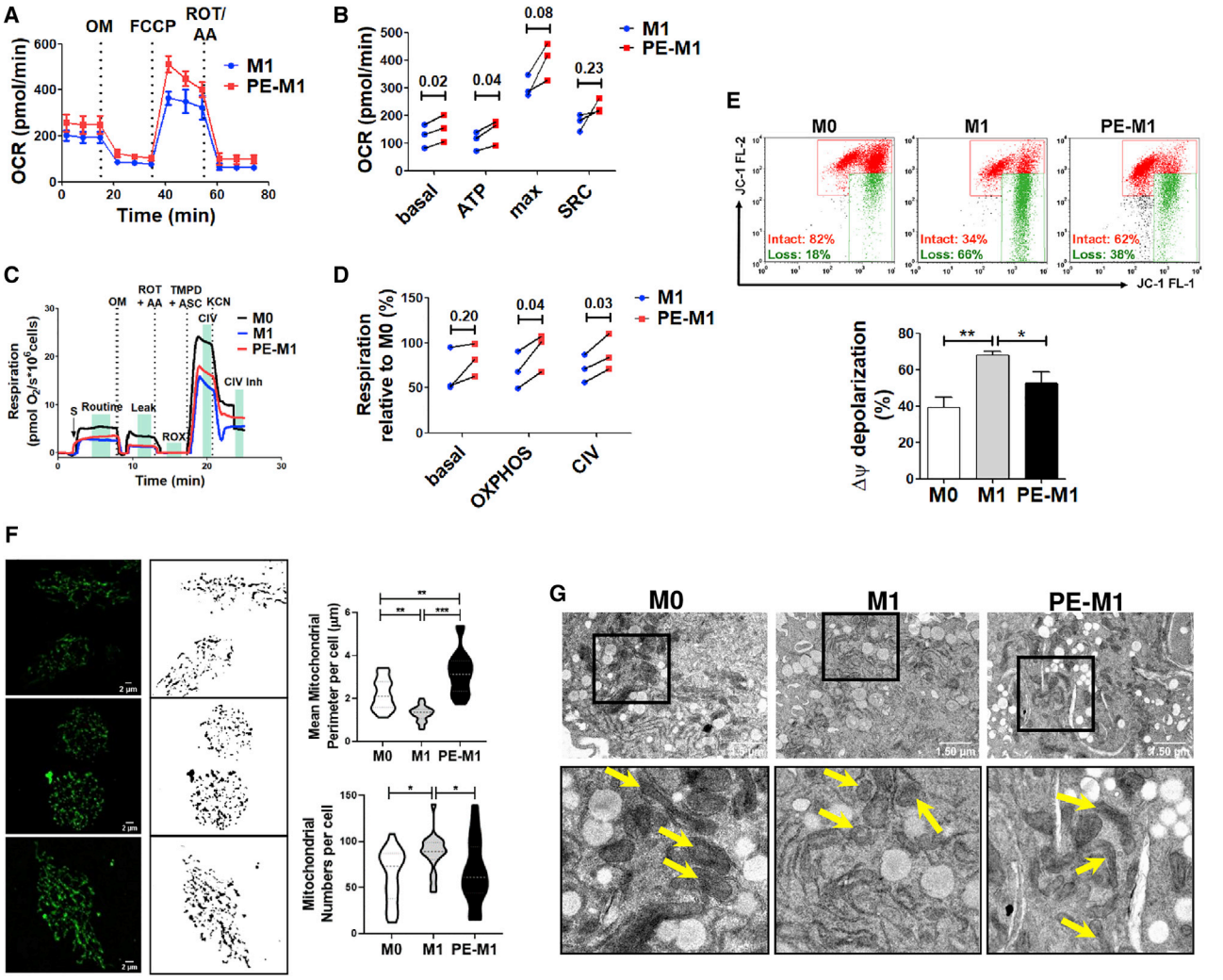

Figure 2. TB-PE Prevents Mitochondrial Dysfunctions Characteristic of M1 Macrophages

(A–D) OXPHOS parameters assessed by recording the OCR values using a Seahorse Analyzer (A and B) or an Oroboros Oxygraphy-2K (C and D). (A and C) One representative experiment (triplicates). (B and D) Respiratory parameters measured in three independent experiments (paired t tests).

(E) Mitochondrial membrane potential measured by JC-1 probe staining (n = 6). Friedman test followed by Dunn's multiple comparison test (*p < 0.05; **p < 0.01), as depicted by lines. Values are expressed as means ± SEM.

(F) Analyses of mitochondrial morphology by confocal microscopy in macrophages. Representative z stacks of images of green Mitospy-stained macrophages and their corresponding grayscale mask image. Right panels show the mean mitochondrial perimeter and numbers of mitochondria per cell from one out of five representative donors. One-way ANOVA followed by Bonferroni's multiple comparison test (*p < 0.05; **p < 0.01; ***p < 0.001), as depicted by lines.

(G) Representative electron microscopy micrographs of macrophages showing mitochondrial ultrastructure. Yellow arrows denote mitochondria.

predominant isoform in M1 macrophages (Boscá et al., 2015). The upregulation of both enzymes seen in M1 was lower or absent, respectively, in PE-M1 (Figures 1H). Altogether, these results indicate that soluble factors generated by Mtb infection can inhibit the glycolytic metabolic potential of human macrophages during their differentiation toward the microbicidal program.

TB-PE Prevents Mitochondrial Dysfunctions Characteristic of M1 Macrophages

To further understand the metabolic rewiring induced by TB-PE, we evaluated the mitochondrial function in macrophages by measuring the oxygen consumption rate (OCR) using two different experimental approaches, namely the sensitive high-throughput Seahorse Extracellular Flux Analyzer (Figures 2A and 2B) and the high-resolution Oxygraph-2k (Figures 2C and 2D). Both methodologies clearly demonstrated that PE-M1 macrophages have enhanced OXPHOS compared to M1 cells (Figures 2A–2D). In fact, PE-M1 macrophages displayed higher basal respiration and ATP-linked OCR (Figures 2A and 2B), as well as higher OXPHOS-linked OCR and complex IV activity (Figures 2C and 2D), than M1 macrophages. The decrease in the TCA cycle and electron transport taking place in these cells is known to lead to a reduction in the mitochondrial membrane

potential (Palsson-McDermott and O'Neill, 2013). Therefore, we assessed the effect of TB-PE on the mitochondrial inner membrane potential. M1 cells displayed a higher percentage of cells with reduced membrane potential than M0 macrophages, while the TB-PE treatment prevented this increase (Figure 2E).

Mitochondrial shape and bioenergetics are intimately linked (Rambold and Pearce, 2018), and mitochondrial morphology is altered in macrophages stimulated with LPS, leading to small, diverse mitochondria dispersed throughout the cytoplasm (Gao et al., 2017). Confocal microscopy of macrophages labeled with Mitospy, which stains mitochondria regardless of their membrane potential, revealed punctate and more numerous mitochondria in M1 macrophages, while in PE-M1 cells the organelles were more tubular and less numerous, similar to M0 cells (Figure 2F). Transmission electron microscopy confirmed that compared to M0 cells, mitochondria in M1 macrophages were smaller and displayed a disrupted cristae shape, while these defects were not seen in PE-M1 cells (Figure 2G). These findings support the hypothesis that soluble factors generated during Mtb infection block the shift toward the aerobic glycolysis that is usually accompanied by mitochondrial dysfunction during the activation of microbicidal macrophages.

TB-PE Inhibits HIF-1α Expression and Pro-inflammatory Functions in M1 Macrophages

To address potential mechanisms underlying the inhibitory effects of TB-PE, we evaluated the expression of HIF-1α. Indeed, HIF-1α was induced in M1 cells, but not in PE-M1 cells, at the protein and RNA level (Figures 3A and 3B). Unlike PEs from heart failure patients, a second PE pool or multiple individual PE samples from TB patients inhibited the upregulation of HIF-1α in M1 macrophages (Figure 3C). An important enhancer of HIF-1α activity is the mammalian target of rapamycin (mTOR) complex 1 (mTORC1). HIF-1α can be activated by mTORC1 upon cytokine signaling, elevated levels of succinate, or reactive oxygen species (ROS) (Finlay et al., 2012; Movafagh et al., 2015; Tannahill et al., 2013). Upon activation, mTOR is phosphorylated on several residues, including S2448; while we found that this phosphorylated form was upregulated in M1, we failed to detect it in PE-M1 cells (Figure 3D). Bacterial infection or LPS stimulation, results in increased nuclear factor κB (NF-κB) activity in phagocytes, which in turn induces *HIF-1α* mRNA transcription (Rius et al., 2008). Pro-inflammatory features such as the expression of NF-κB, the release of IL-1β, and the production of mROS were less prominent in PE-M1 than M1 cells (Figures 3E–3G). Noticeably, we verified that IL-1β production by M1 macrophages was reproducibly inhibited after treatment with different independent pools of TB-PE, unlike that from heart failure patients (Figure 3H). Hence, the soluble factors generated by Mtb infection exert their inhibitory effect on pro-inflammatory functions as well as HIF-1α activity.

TB-PE Inhibits Pro-inflammatory Functions in Human Macrophages in Response to Mtb

Mtb infection leads to glycolysis in bone-marrow-derived macrophages (Koo et al., 2012; Mehrotra et al., 2014) and increased HIF-1α expression in IFN-γ-activated macrophages (Braverman et al., 2016). We confirmed this is also the case in IFN-γ-polarized macrophages stimulated with irradiated Mtb or infected with live Mtb, since both lactate release and HIF-1α expression increased (Figures 4A–4D). In fact, different strains of Mtb displayed similar capacity to induce the metabolic reprogramming in IFN-γ-polarized macrophages, as measured by lactate release and glucose consumption (Figures S2A and S2B). Importantly, TB-PE treatment reduced the release of lactate and the expression of HIF-1α driven by irradiated or live Mtb (Figures 4A–4D). This effect is not due to cell death induced by TB-PE treatment, as we monitored cell viability in macrophages at 48 h post-infection and found no changes compared with untreated cells (Figure S2C). Furthermore, HIF-1α-associated production of mROS and IL-1β in response to irradiated Mtb was reduced in PE-treated macrophages (Figures 4E and 4F). Of note, while no differences in Mtb internalization were observed among the different groups of macrophages at day 0, PE-treated cells showed an increase in live Mtb load at days 3 and 6 post-infection, thus reflecting a lower microbicidal activity (Figures 4G and S2D). Concerning surface marker expression, macrophages stimulated with IFN-γ and irradiated Mtb upregulated the levels of HLA-DR, CD86, PD-L1, and CD80, regardless of TB-PE treatment (Figures S2E and S2F). These observations establish that beyond the classical activation of macrophages with IFN-γ/LPS, soluble factors generated by Mtb infection can also inhibit the activation of pro-inflammatory and metabolic properties in these cells interacting directly with the pathogen.

HIF-1α Stabilization Reverts the Inhibitory Effects of TB-PE on the Pro-Inflammatory Macrophage Program

To establish the role of HIF-1α as the target of the TB-PE treatment, we stabilized its activity by blocking the HIF prolyl hydroxylases (Jaakkola et al., 2001). To this end, we used inhibitors of prolyl hydroxylases, such as dimethyloxalylglycine (DMOG) and cobalt (II) chloride ($CoCl_2$). HIF-1α stabilization in PE-M1 cells treated with DMOG or $CoCl_2$ resulted in higher expression of HIF-1α, HK2 and LDHA, as well as an increase in lactate production and in mitochondrial fragmentation and cristae defects (Figures 5A–5E). Of note, *LDHA* and *HK2* are target genes under the transcriptional control of HIF-1α (Boscá et al., 2015; Semba et al., 2016). These phenotypic changes induced by HIF-1α stabilization were associated with the recovery of pro-inflammatory functions, such as IL-1β and mROS production (Figures 5F and 5G). Along with these functional changes, TB-PE also promoted a poor capacity to control the bacillary load in IFN-γ-activated macrophages, a feature that was reverted by DMOG treatment (Figures 5H and 5I). In order to shed light into the mechanism by which DMOG improves the microbicidal activity of Mtb-infected M1 cells exposed to TB-PE, we inhibited different molecules related to IL-1β secretion, such as caspases, ROS, and IL-1 receptors (IL-1Rs), and assessed their impact on the bacillary loads (Figure S3A). Accordingly, we observed that the blocking of IL-1R using a specific antibody significantly increases mycobacterial growth in DMOG-treated PE-M1 cells (Figure 5J). In addition, there is a complete IL-1β secretion inhibition in M1 macrophages exposed to either caspase or ROS inhibitors (Figure S3B). In line with these findings, we also found that the caspase and ROS inhibition impairs the ability of PE-M1 macrophages treated with DMOG to control Mtb intracellular growth (Figure 5J). All in all,

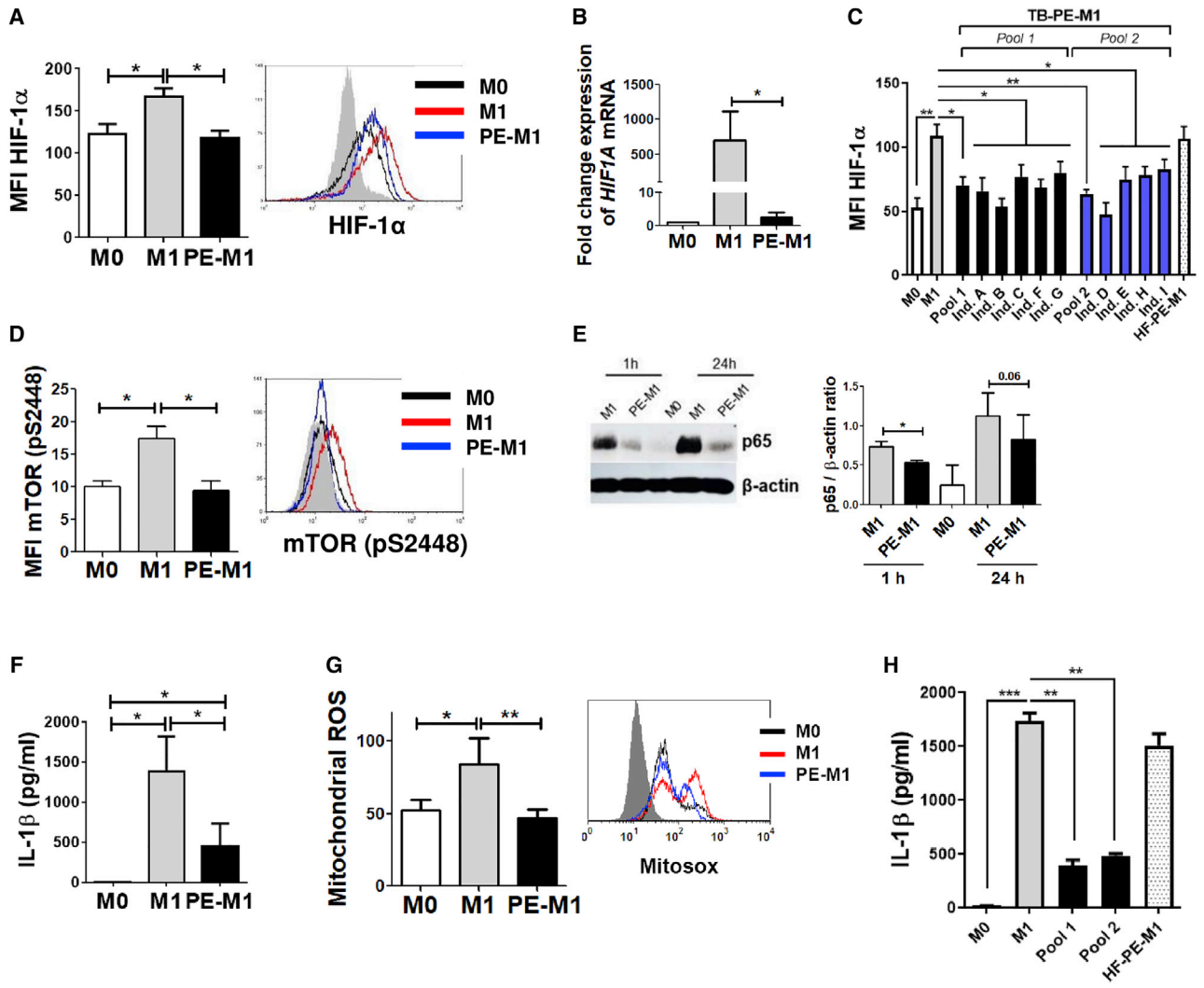

Figure 3. TB-PE Inhibits HIF-1α Expression and Pro-inflammatory Functions in M1 Macrophages

(A) Left: mean fluorescence intensity (MFI) of HIF-1α measured by FACS (n = 7). Right: representative histogram.

(B) Expression of *HIF-1α* mRNA relative to M0 (n = 6).

(C) HIF-1α expression in macrophages (M0) polarized toward the M1 profile with LPS and IFN-γ in the presence (TB-PE-M1) or absence (M1) of the acellular fraction of two different pools of TB-PEs (prepared with samples from 10 different patients each), with individual TB-PE from single patients (Ind. A to Ind. I) or a pool of pleural effusions from patients with heart failure (HF-PE-M1). n = 4.

(D) Left: percentages of mTOR-(pS2448)-positive cells measured by FACS (n = 5). Right: representative histogram.

(E) Analysis of p65 and β-actin protein expression level at 1 and 24 h post-stimulation by western blot (left panel) and quantification (right panel; n = 4) macrophages.

(F) IL-1β production by ELISA (n = 4).

(G) Left: MFI quantification of MitoSOX for human macrophages (n = 12). Right: representative histogram.

(H) IL-1β production by M1 macrophages exposed to two different pools of TB-PE (n = 6).

Friedman test followed by Dunn's multiple comparison test (*p < 0.05; **p < 0.01), as depicted by lines. Values are expressed as means ± SEM.

these data establish a central role for the inhibition of HIF-1α activity in the impaired microbicidal activity of macrophages triggered by soluble factors generated during Mtb infection.

HIF-1α Stabilization Improves Mycobacterial Control in Mice and Is Associated with Mitochondrial Stress in AMs

Next, we evaluated the effect of DMOG on the bacillary loads and on the mitochondrial functions of pulmonary macrophages from Mtb-infected mice treated (or not) with DMOG at early stages of Mtb infection. DMOG-treated mice had lower pulmonary bacillary loads at 14 days post-infection than control mice (Figure 6A). We then followed a flow cytometric gating protocol based on previous analysis to distinguish different types of mononuclear phagocytes present in lungs of Mtb-infected mice (Huang et al., 2018) (Figure S4A). DMOG-treated mice had a higher percentage (but not a higher absolute number) of

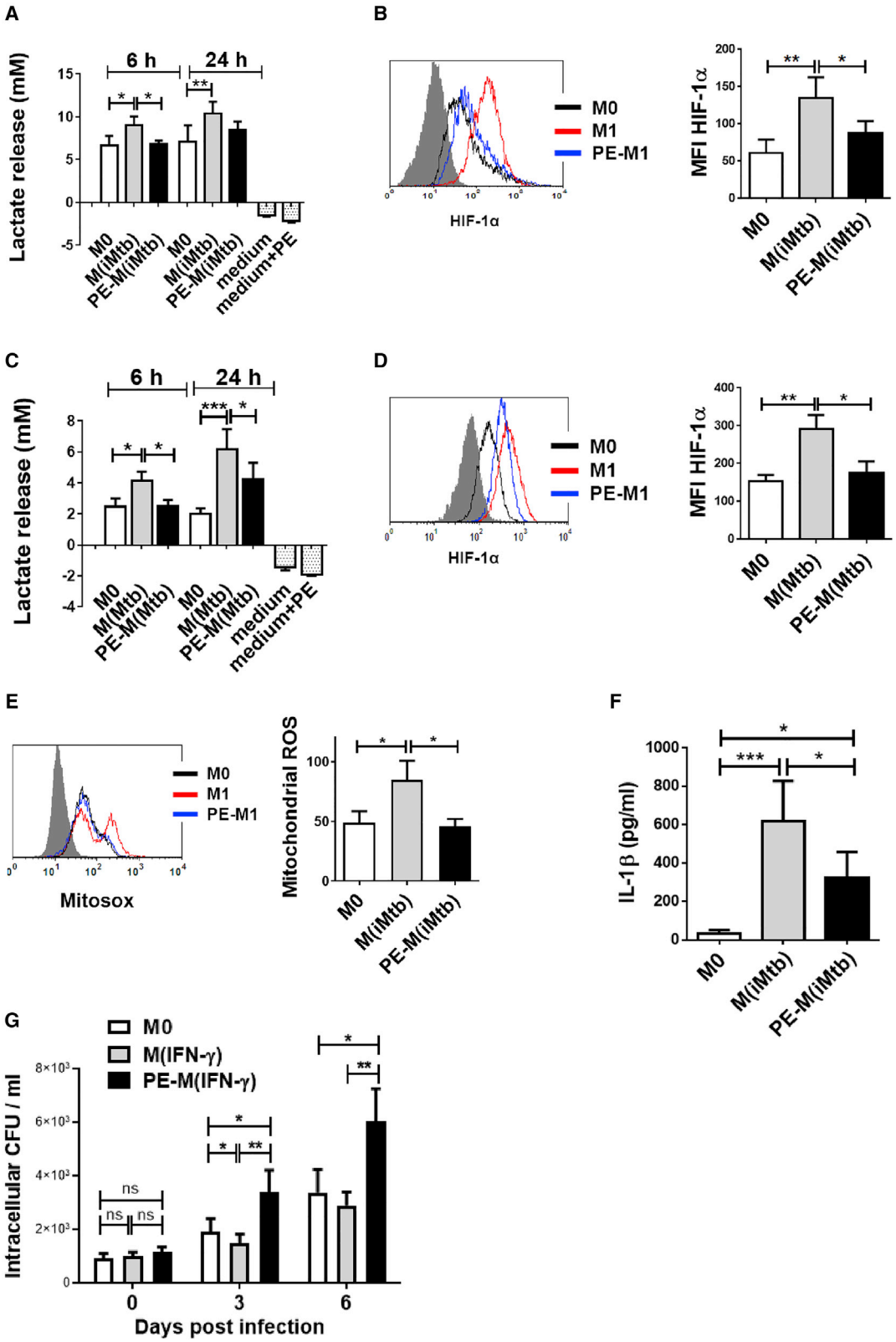

(legend on next page)

AMs than control mice (Figures 6B and 6C). No significant differences were found in the percentage or absolute number of IMs (Figures 6D and 6E) or lung polymorphonuclear leukocytes (Figures S4B and S4C). In addition, both AMs and IMs from DMOG-treated animals had lower mitochondrial inner membrane potential (Figures 6F and S4D–S4F) and higher mROS production than control AMs (Figures 6G and S4G–S4I).

Since HIF-1α stabilization enhances IL-1β production and this cytokine was shown to promote the translocation of infected AM from the alveoli into the lung interstitium (Cohen et al., 2018), we assessed whether the distribution of AM was affected within lung compartments of DMOG-treated animals. Histological analysis of infected mice with the Mtb strain constitutively expressing mCherry showed no difference in the absolute total number of Siglec-F$^+$ macrophages, considering both the alveolar and interstitial space recovered from control and DMOG-treated mice (Figure 6H). By contrast, the distribution of these cells in the alveolar compartment was modified relative to the interstitial space (Figure 6I). Indeed, while DMOG increases the percentage of Siglec-F$^+$ macrophages in the interstitial space, it also reduces their presence in the alveoli compared to the incidence found in control mice (Figures 6I and 6J). Moreover, the interstitial cells positive for Siglec-F appeared to contain Mtb in DMOG-treated mice (Figure 6J), indicating that HIF-1α stabilization at the early stage of infection increases translocation of Mtb-containing macrophages to the lung interstitium.

These results indicate that DMOG treatment can protect against Mtb infection, and this protection is associated with an increase in AM mitochondrial stress, suggesting a metabolic switch.

Involvement of Host-Derived Lipids from TB-PE in the Metabolic Remodeling Activity of M1 Macrophages

To investigate the nature of the TB-PE components responsible for the metabolic alterations observed in human macrophages, we tested the metabolic activity of the TB-PE fraction obtained after treatment with proteinase K, which was embedded onto polyacrylamide hydrogel (Pk-PE). Protein digestion was controlled using SDS-PAGE, followed by Coomassie blue staining (Figure S5A). TB-PE digested of proteins was still able to diminish the release of lactate driven by IFN-γ/LPS without inducing cell death in M1 macrophages (Figures S5B and S5C). Thereafter, we separated two fractions of TB-PE, one enriched in polar metabolites (PMPEs) and the other comprising lipids (LPEs), and used them to treat M1 macrophages at the same concentration as in the untouched TB-PE (1x) or at a double dose (2x). LPEs, but not PMPEs, was able to reduce the release of lactate at comparable doses found in intact TB-PE (Figure 7A). Cell viability was not modified either by PMPE or LPE treatment at 1x or 2x doses (Figures 7B and S5D). In line with the reduction of lactate, LPEs also inhibited HIF-1α expression (Figure 7C), partially decreased mROS production by M1 macrophages (Figure 7D), and rendered the IFN-γ-activated macrophages more susceptible to Mtb intracellular growth (Figure 7E).

To determine whether metabolic-active lipids found in TB-PE were bacterial or host derived, we performed a lipidomic analysis of the LPE. Mass spectrometry signals corresponding to the main mycobacterial lipid families were not detected in the TB-PE lipid extract dataset (Figure S6A) according to MycoMass and MycoMap databases (Layre et al., 2011), supporting the idea that the activity of TB-PE lipid extract is likely to be driven by host lipids. This notion was further supported by the fact that the total lipid fraction obtained from Mtb was not able to impair the release of lactate by M1 macrophages in our experimental settings (Figures 7F and S6B). These results support the notion that host-derived lipid components elicited by Mtb infection are responsible for rewiring the metabolism of M1 macrophages impacting the control of the bacillary intracellular load.

Next, we focused our attention on eicosanoids, the host-derived lipid class best known to be involved in the modulation of inflammation (Dennis and Norris, 2015). To this end, we assessed the impact of the eicosanoid-enriched fraction of TB-PE on the metabolism and activation status of M1 macrophages. As illustrated in Figure 7G, the release of lactate and IL-1β, as well as HIF-1α expression, in M1 macrophages was diminished by the eicosanoid-enriched fraction to the same extent as intact TB-PE. Likewise, the eicosanoid-enriched fraction of TB-PE rendered M1 macrophages more susceptible to Mtb intracellular growth (Figure 7H). Finally, we characterized eicosanoids extracted from TB-PE pool by high-end mass spectrometry and performed their absolute quantification, as previously described (Le Faouder et al., 2013). As illustrated in Figure 7I, we observed that almost all detected eicosanoids are enriched in TB-PE compared to the heart failure patient PE pool. Additionally, we determined the absolute quantification of eicosanoid species in three individual samples of TB-PE and in two different pools of TB-PE and applied principal-component analysis (PCA) to explore the tendency of separation among samples confirming the enriched presence of these lipid mediators (as compared to pleural effusions from patients with heart failure [HF-PE] control) (Figure 7J). Altogether, these results strongly suggest that

Figure 4. TB-PE Inhibits Pro-inflammatory Functions in Human Macrophages in Response to Mtb

GM-CSF-driven human macrophages (M0) were stimulated with IFN-γ and irradiated Mtb or live Mtb in the presence (PE-M(iMtb) and PE-M(Mtb)) or absence (M(iMtb) and M(Mtb)) of the acellular fraction of TB-PEs.

(A and C) Lactate release by macrophages in responses to stimulation or not with irradiated (A) or live (C) Mtb in the presence or absence of PE at 6 and 24 h; n = 8 (A) and n = 9 (C).

(B and D) Mean fluorescence intensity (MFI) of HIF-1α induced by irradiated (B) or live (D) Mtb at 24 h; n = 7 (B) and n = 8 (D).

(E) MFI quantification of MitoSOX for human macrophages in responses to stimulation or not with irradiated Mtb H37Rv in the presence or absence of PE at 24 h (n = 5).

(F) IL-1β cytokine levels produced by macrophages in responses to stimulation or not with irradiated Mtb H37Rv in the presence or absence of PE at 24 h (n = 5).

(G) Intracellular colony-forming units (CFUs) were determined at different time points in macrophages (M0) stimulated with IFN-γ in the presence (PE-M(IFN-γ)) or absence (M(IFN-γ)) of PE for 24 h, washed, and infected with Mtb (n = 7). Uptake of Mtb was determined by evaluating the CFU at 4 h post-infection (day 0). Friedman test followed by Dunn's multiple comparison test (*$p < 0.05$; **$p < 0.01$; ***$p < 0.001$) as depicted by lines. Values are expressed as means ± SEM.

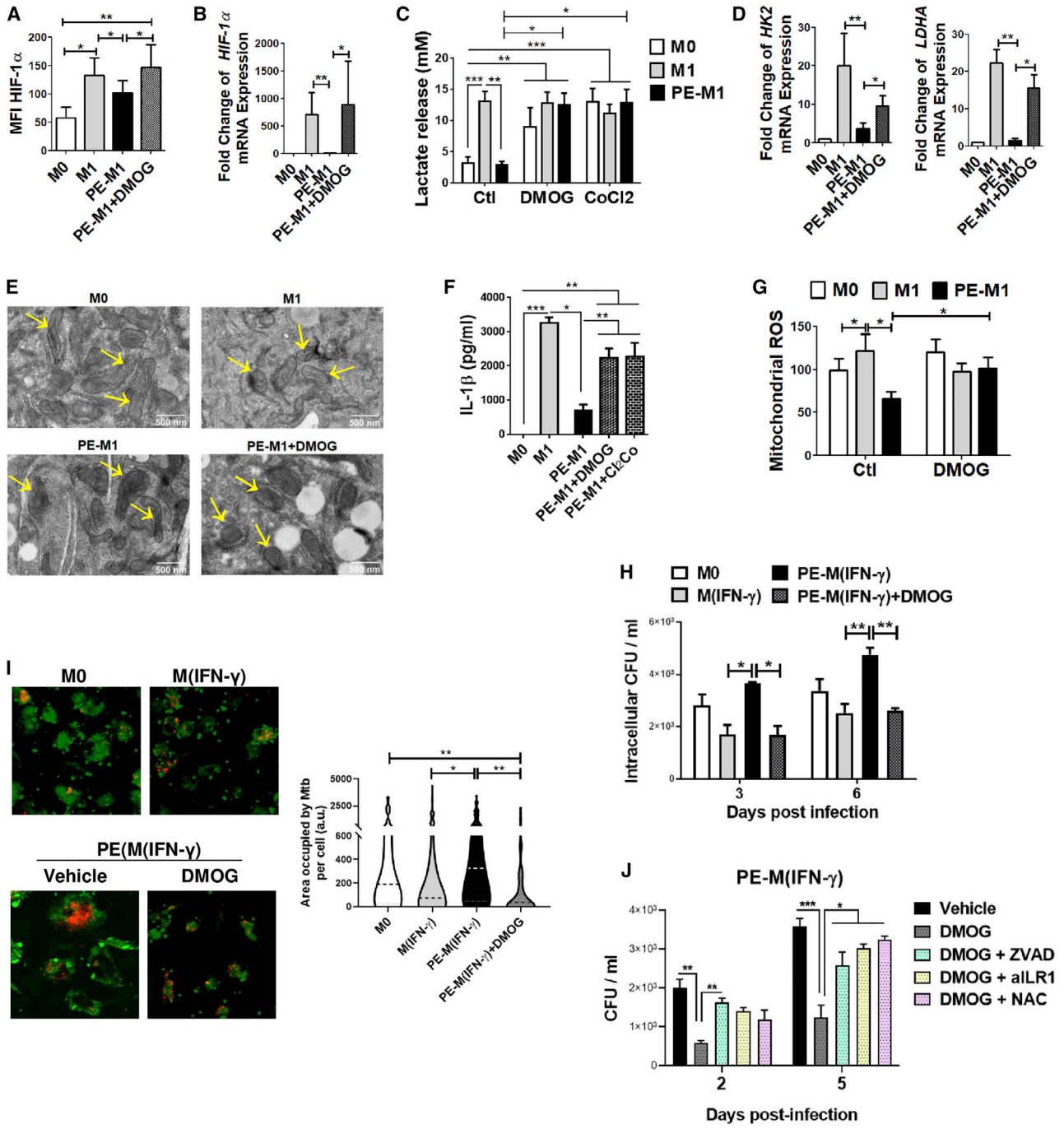

Figure 5. HIF-1α Stabilization Reverts the Inhibitory Effects of TB-PE on the Pro-inflammatory Macrophage Program

GM-CSF-driven human macrophages (M0) were polarized toward the M1 profile with LPS and IFN-γ in the presence (PE-M1) or absence (M1) of the acellular fraction of TB-PEs with or without DMOG or $CoCl_2$. (A) HIF-1α expression in macrophages (n = 7).

(B) Expression of *HIF-1α* mRNA relative to M0 (n = 6).

(C) Lactate release by macrophages (n = 6).

(D) Expression of *LDHA* mRNA and hexokinase 2 (*HK2*) mRNA relative to M0 (n = 7).

(E) Representative electron microscopy micrographs of macrophages showing mitochondrial ultrastructure. Yellow arrows denote mitochondria.

(F) IL-1β production by ELISA (n = 7).

(G) MFI quantification of MitoSOX for human macrophages (n = 7).

(H) M0 and IFN-γ-activated macrophages were infected with Mtb and exposed or not to TB-PE and DMOG. Intracellular CFUs were determined at different time points (n = 4). Friedman test followed by Dunn's multiple comparison test (*$p < 0.05$; **$p < 0.01$), as depicted by lines.

(legend continued on next page)

eicosanoids present in TB-PE may mediate the metabolic alterations taking place M1 macrophages exposed to this TB microenvironment.

DISCUSSION

TB, as a chronic condition, entails the establishment of extensive metabolic remodeling in both host and pathogen (Russell et al., 2010). Our ability to control the burden of TB globally is limited by the absence of an effective vaccine, an aspect that is worsened by the lack of any reliable immune correlates of local tissue protective immunity (Bhatt and Salgame, 2007; Goletti et al., 2016; Huang and Russell, 2017). Therefore, more basic research focused on human physiologically relevant samples derived from active TB patients is required to perform functional and mechanistic studies on TB under physiological conditions. In this regard, numerous studies have focused on the investigation of the broncho-alveolar lavage and, relatively less frequently, of lung tissue explants obtained from patients undergoing lung surgery for clinical reasons unrelated to pulmonary infection, which were infected *in vitro* with Mtb (Ganbat et al., 2016; Maertzdorf et al., 2018). In the former case, to obtain the broncho-alveolar lavage, a saline solution must be instilled in the lung, causing the unavoidable dilution of the lung milieu. In addition, broncho-alveolar lavages usually result in an incomplete sample and poor representative of the lower lung airways; it is also an invasive and risky procedure, making subjects less reluctant to participate. In the latter case, there is no leukocyte recruitment to the site of infection. In comparison, as a therapeutic procedure to drain the effusion for clinical diagnosis that also improves patient clinical conditions, we argue that PE is an unperturbed microenvironment generated by Mtb infection and contains most of the leukocyte populations that are involved in TB immunity, including monocytes and macrophages. Although we are aware that *ex vivo/in vitro* studies do not fully reflect the complexity of the lung architecture and its impact on host-pathogen interactions, the use of the acellular fraction of the infection site provides a unique tool to study how a bona fide TB-associated pleural milieu influences the host cells. In this regard, we have previously used the acellular fraction of TB-PE and demonstrated its pertinence as a model human lung TB microenvironment (Genoula et al., 2018; Lastrucci et al., 2015; Souriant et al., 2018).

Here, we show that host-derived lipids, particularly an eicosanoid-enriched fraction within the acellular TB-PE, alter the metabolic reprogramming of M1 macrophages by targeting HIF-1α expression. In our experimental model, we exposed granulocyte-macrophage colony-stimulating factor (GM-CSF)-driven human macrophages to M1-activating stimuli in the presence (or not) of the TB-PE to better reflect the complex milieu in which the activation program may take place physiologically. Even though GM-CSF itself skews macrophages toward glycolysis (Na et al., 2017), we considered these as "M0" cells to emphasize their lower activation state in comparison to those stimulated with LPS or Mtb. Yet, these cells are very different from the classical "M0" generated under macrophage colony-stimulating factor (M-CSF) treatment (Jaguin et al., 2013). In terms of metabolic parameters, we demonstrated that even when PE-M1 macrophages showed a higher consumption of glucose, this additional glucose is not converted into lactate, as in M1 cells, but rather is used to feed the OXPHOS pathway, adopting an M2-like metabolic profile. In this regard, although it was widely accepted that a higher consumption of glucose associates with M1 macrophages, leading to higher aerobic glycolytic activity, it is now known that M2 macrophages (e.g., driven by IL-4) also exhibit enhanced glucose utilization during their activation program; higher glucose uptake is used to feed mitochondrial respiration (Huang et al., 2016). In line with this, TB-PE-M1 macrophages, shown to be more prone to OXPHOS than M1 cells, also displayed an enhanced consumption of glucose. The less glycolytic profile established in PE-M1 macrophages is further supported by reduced levels of lactate and decreased expression of LDHA and HK2, both HIF-1α target genes (Boscá et al., 2015; Semba et al., 2016). Additionally, we demonstrated that TB-PE impairs M1-associated metabolism, but it also leads to a mixed repertoire of cell-surface markers in macrophages, reflecting the complex nature of TB-PE as a physiologically relevant fluid.

Another line of supporting evidence for the capacity of TB-PE to influence the metabolic state of microbicidal macrophages is the change in mitochondrial morphology that is compatible with a more active oxidative metabolism, such as (1) tubular mitochondria and (2) functional cristae with folding architecture of the mitochondrial inner membrane. The fusion process between mitochondria is important for OXPHOS activity, while the fission process leads to a higher number of smaller and punctuated organelles, which have impaired mitochondrial respiration activity (Rambold and Pearce, 2018). In this regard, LPS-stimulated macrophages have small, diverse mitochondria dispersed throughout the cytoplasm (Gao et al., 2017), which we confirmed in our IFN-γ/LPS-stimulated macrophages. This mitochondrial fragmentation observed in M1 macrophages is not achieved when cells are exposed to TB-PE. Also, changes in the ultrastructure of mitochondria are associated with the regulation of mitochondrial functions; that is, mitochondrial cristae are the main site of OXPHOS, and their folded structure is critical for respiratory chain supercomplex assembly (Cogliati et al., 2016). In this context, we showed a normalization of mitochondrial cristae morphology in PE-M1 cells compared with M1 macrophages, which is consistent with the elevated OXPHOS activity found in

(I) M0 and IFN-γ-activated macrophages were infected with RFP-expressing Mtb and exposed or not to TB-PE and DMOG. The area occupied by Mtb per cell was assessed in z stacks from confocal laser scanning microscopy images at 48 h post-infection. One representative experiment showing 80–100 cells per condition is shown. One-way ANOVA followed by Bonferroni's multiple comparison test (*$p < 0.05$ and **$p < 0.01$), as depicted by lines.
(J) Left: TB-PE-treated IFN-γ-activated macrophages (PE-M(IFN-γ) were infected with Mtb and exposed (or not) to DMOG with pan caspase inhibitor Z-VAD-FMK (ZVAD), N-acetyl-l-cysteine (NAC), or IL-1 receptor antagonist (aIL1R). Intracellular CFUs were determined at different time points ($n = 6$). Friedman test followed by Dunn's multiple comparison test (*$p < 0.05$; **$p < 0.01$) for treatment versus PE-M1(IFN-γ) + DMOG. Right: scheme showing the molecular pathways inhibited by the different drugs in M1 macrophages. Values are expressed as means ± SEM.

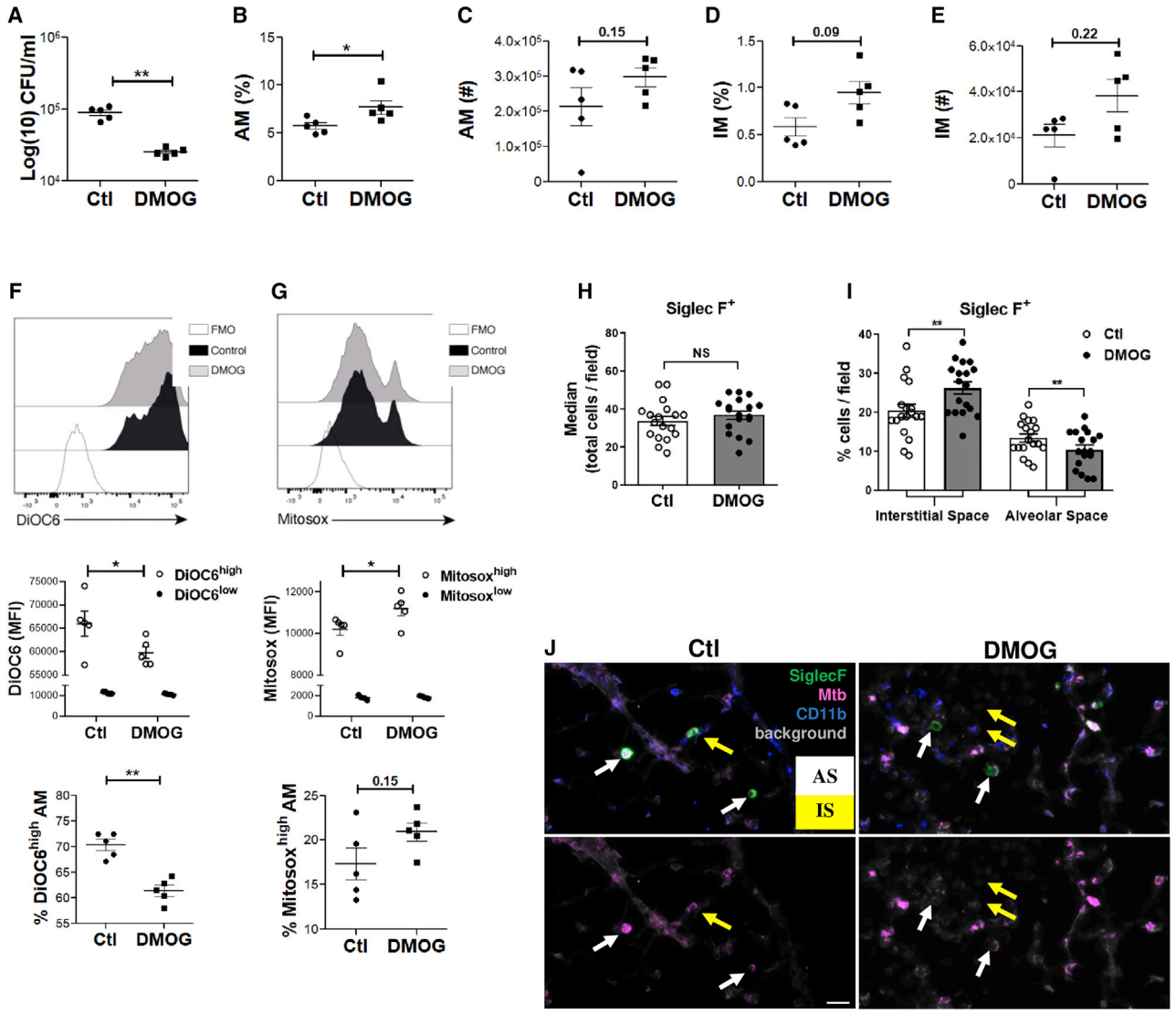

Figure 6. HIF-1α Stabilization Improves Mycobacterial Control in Mice and Is Associated with Mitochondrial Stress in AMs

Mice were infected intranasally with Mtb (1,000 CFU per mouse) and then treated or not with DMOG for 14 days.

(A) CFUs recovered from lungs of DMOG-treated mice or control mice (Ctl). A representative experiment of three independent experiments is shown.

(B and C) Percentages of AMs among CD45.2$^+$ live cells (B) and absolute number of AMs (C). A representative of two independent experiments is shown.

(D and E) Percentages of IMs among CD45.2$^+$ live cells (D) and absolute number of AMs (E). A representative experiment of two independent experiments is shown.

(F) Top: representative histogram of DiOC6 labeling for AMs from DMOG-treated mice, control mice, and fluorescent minus one (FMO). Vertical dashed line separates high versus low events. Intermediate panel: Mean fluorescent intensity (MFI) quantification of DiOC6 for AM. Bottom: percentages of DiOC6^{high} AMs. A representative of two independent experiments is shown.

(G) Top: representative histogram of MitoSOX labeling for AMs from DMOG-treated mice, control mice, and FMO. Middle: MFI quantification of MitoSOX for AMs. Vertical dashed line separates high versus low events. Bottom: percentages of MitoSOX^{high} AMs. A representative of two independent experiments is shown.

(H–J) Lungs from Mtb-infected mice treated (or not) with DMOG were harvested 2 weeks after infection, and SIGLEC-F antibodies were instilled intranasally 30 min prior to their sacrifice. The lungs were fixed, dehydrated, embedded in OCT, and sectioned before histological analysis. (H) Total number of Siglec-F$^+$ macrophages per field was quantified (10×), with six fields per mice (n = 3). (I) Percentages of Siglec-F$^+$ macrophages in the alveolar or interstitial space per field were quantified. (J) Representative histological images of control and DMOG-treated mice lungs (40×). Siglec-F$^+$ macrophages are shown in green, CD11b$^+$ total macrophages in blue, Mtb-mCherry in magenta, and the tissue in white (tissue autofluorescence). White arrows show Siglec-F$^+$ macrophages in the alveolar space (AS), and yellow arrows show Siglec-1$^+$ macrophages in the interstitial space (IS). Scale bar, 20 μm. Mann-Whitney test (*p < 0,05; **p < 0,01) or two-way ANOVA (*p < 0.05).

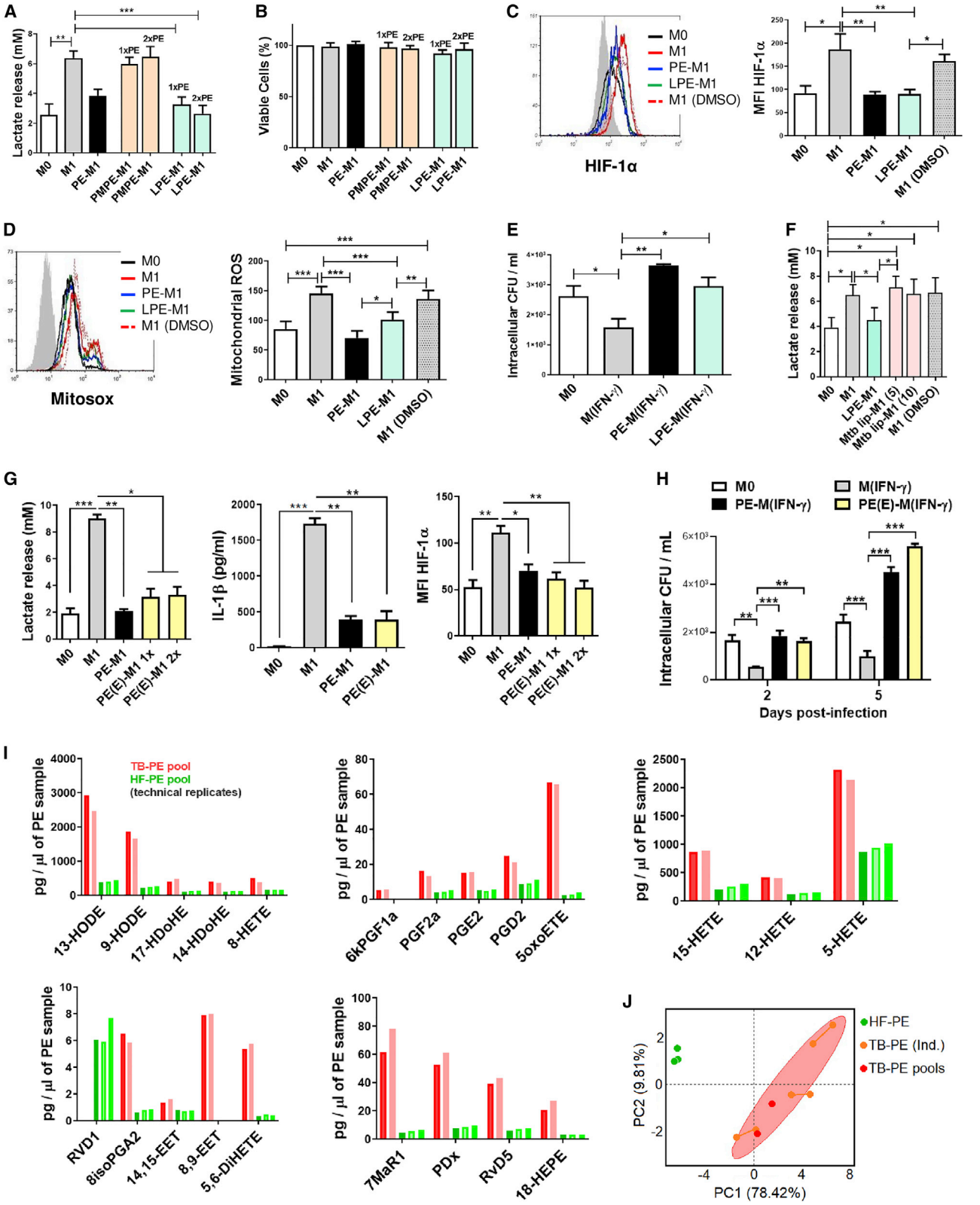

(legend on next page)

PE-M1 cells. Particularly, the loss of mitochondrial membrane potential is associated with accumulation of mROS (Cai et al., 2015; Ip et al., 2017; Weinberg et al., 2015). Also, mitochondrial depolarization is central to the increased microbicidal ability of macrophages under hypoxia or upon activation in response to Mtb infection (Matta and Kumar, 2016). In agreement with these findings, PE-M1 macrophages exhibited neither loss of mitochondrial membrane potential nor an appreciable induction of mROS upon LPS stimulation, displaying impaired ability to control Mtb intracellular load. Metabolic repurposing of mitochondria away from OXPHOS is key to the regulation of pro-inflammatory responses, including the expression of pro-IL-1β and the generation of mROS via reverse electron transport (Van den Bossche et al., 2017). Indeed, the pro-inflammatory cytokine IL-1β is a crucial mediator of inflammation and plays a vital role in the host resistance to Mtb infections (Juffermans et al., 2000). In our study, we demonstrated that molecular pathways leading to IL-1β secretion and function are necessary to control the mycobacterial intracellular growth in macrophages. In the case of mROS, it is thought that professional phagocytes generate ROS primarily via the phagosomal nicotinamide adenine dinucleotide phosphate (NADPH) oxidase machinery, contributing to macrophage bactericidal activity (West et al., 2011). mROS can be delivered to *Staphylococcus-aureus*-containing phagosomes via mitochondria-derived vesicles (Abuaita et al., 2018), providing a putative explanation for how mROS can reach bacteria within the phagosomal lumen. Regardless of the direct microbicidal effect of mROS, these species can also contribute to the pro-inflammatory profile by promoting the expression of HIF-1α (Wang et al., 2010).

HIF-1α and mTOR are now recognized as the key regulators of this shift of metabolism toward glycolysis (Srivastava and Mannam, 2015). We found that the stabilization of HIF-1α using DMOG restores the M1 functions in PE-M1 macrophages. While DMOG treatment is known to increase HIF-1α protein levels, we also observed an increase in mRNA expression. As a positive feedback loop between HIF-1α and aerobic glycolysis has been reported (Braverman et al., 2016), we consider that recovering the glycolytic flux in DMOG-treated PE-M1 macrophages can increase HIF-1α expression at both the transcriptional and post-transcriptional levels.

Within the context of TB, eicosanoids are present in PE and plasma of infected patients (el-Ahmady et al., 1997; Pace et al., 2004; Pavan Kumar et al., 2019), and genetic polymorphisms in some enzyme involved in eicosanoid synthesis are associated with susceptibility to human pulmonary TB (Herb et al., 2008; Narendran et al., 2016; Rito et al., 2019). Moreover, these lipid mediators are also known to act in a pro- or anti-inflammatory ways and regulate the replication of Mtb *in vitro* in macrophages and *in vivo* in animal models (Arnett et al., 2018; Bafica et al., 2005; Chen et al., 2008; Mishra et al., 2017; Tobin et al., 2012, 2013). Of note, some of the most abundant eicosanoids species (e.g., 13-hydroxyoctadecadienoic acid [13-HODE]) present in the TB-PE are known to modulate the fate of human macrophages (e.g., decrease of mROS) similarly to TB-PE extract (Fischer et al., 2002). In this study, we provide strong arguments for the notion that the active lipids in TB-PE are not of mycobacterial origin, such as (1) the paucibacillary nature of TB-PE; (2) the fact that Mtb total lipid extract, which contains both characterized and uncharacterized lipids, did not impair the release of lactate by M1 macrophages; and (3) the absence of mass spectrometry signals in TB-PE corresponding to the main mycobacterial lipid families. Notwithstanding, we cannot exclude an alternative (albeit unlikely) possibility concerning the presence of an annotated mycobacterial lipid (not included in our targeted lipidomic analysis) produced only in the context of an *in vivo* infection that may be responsible for the phenomena in question.

Despite the potential of our findings, some concerns remain to be addressed, including (1) whether TB-PE truly reflects what happens in pulmonary tissue or whether it only represents the situation found in extrapulmonary TB, (2) which eicosanoids present in TB-PE are involved in the described processes, and (3) the timing and duration of the metabolic changes observed in macrophages in the course of the infection. With regard to the accuracy of the TB-PE in recapitulating lung disease, it is worth considering that a diversity of microanatomical compartments and molecular signatures were described in pulmonary lesions from TB patients (Chinta et al., 2018; Marakalala et al., 2016). This suggests that the fate of the infection is determined within each anatomical compartment based on an intrinsic balance between pro- and anti-inflammatory mediators that affect the capacity of the host

Figure 7. Involvement of Host-Derived Lipids from TB-PE in the Metabolic Remodeling Activity of M1 Macrophages

(A and B) Lactate release (A) and cell viability (B) of M0, M1, PE-M1, PMPE-M1 (polar metabolites PE-M1), or LPE-M1 (lipid PE-M1) cells (n = 8). PMPE and LPE fractions were used at the same concentration as in the intact TB-PE (1x) or at a double dose (2×).

(C) HIF-1α expression in macrophages (n = 6).

(D) MFI quantification of MitoSOX for macrophages (n = 8).

(E) M0 and IFN-γ-activated macrophages were infected with Mtb and exposed or not to TB-PE or LPE. Intracellular CFUs were determined at day 3 post-infection (n = 4).

(F) Lactate release by macrophages exposed or not to total lipids fraction obtained from Mtb (Mtb lip) at 5 or 10 μg/mL (n = 6).

(G) Macrophages (M0) were polarized toward the M1 profile with LPS and IFN-γ in the presence of either TB-PE or its eicosanoid-enriched fraction (PE(E)), and lactate release, IL-1β production, and HIF-1α expression were determined (n = 6).

(H) M0 and IFN-γ-activated macrophages were infected with Mtb and exposed (or not) to TB-PE or PE(E). Intracellular CFUs were determined at days 2 and 5 post-infection (n = 6). Friedman test followed by Dunn's multiple comparison test (*$p < 0.05$; **$p < 0.01$; ***$p < 0.001$), as depicted by lines. Values are expressed as means ± SEM.

(I) After addition of internal standards, eicosanoids were extracted from TB-PE and HF-PE pools and analyzed by high-performance liquid chromatography (HPLC) tandem mass spectrometry (MS/MS). Quantification of the different species was calculated based on the chromatogram area ratio between the analyte and its respective internal standard.

(J) Principal-component analysis (PCA) score plot of two different pools of TB-PE, individual TB-PE (three patients with duplicates), and HF-PE samples (triplicates).

to resolve or isolate the pathogen. In this sense, it is plausible that a ratio between pro- and anti-inflammatory eicosanoids may be responsible for the remodeling of the metabolism of macrophages and that the milieu represented in the TB-PE may operate only at the pleural level. Concerning the timing of the metabolic changes induced by Mtb, a recent study demonstrated that, unlike short-term infections, persistent infections with Mtb attenuate glycolysis in macrophages over time (Hackett et al., 2020).

We demonstrated that HIF-1α stabilization improves mycobacterial control in Mtb-infected mice. DMOG promoted M1-like metabolism in tissue-resident AMs, which are known to be biased toward an M2-like phenotype along with susceptibility to intracellular bacterial growth (Huang et al., 2018; Pisu et al., 2020). It is also important to highlight that our results are constrained to early time points of infection (14 days). In fact, it was reported that, unlike early infection, HIF-1α inhibition diminished bacillary loads at later time points, suggesting that sustained activation of HIF-1α may result in pathological inflammation worsening the disease (Baay-Guzman et al., 2018). Interestingly, our findings showing the AM metabolic imprinting by DMOG treatment are complemented by our histological analyses demonstrating a higher capacity of these cells to translocate into the lung interstitium when HIF-1α is stabilized. In this context, Cohen et al. (2018) demonstrated that Mtb-infected AMs migrate from the alveolar space into the interstitium space facilitated by the IL-1R/MyD88-dependent signaling pathway, leading to Mtb dissemination to bystander newly recruited monocytes and neutrophils. In our case, however, this phenomenon might be associated with better control of the infection, possibly due to the antimycobacterial properties promoted by IL-1β signaling. While we cannot exclude that the effects enacted by DMOG treatment are due in part to a pleiotropic effect, we noticed that it does not alter the total numbers of other lung innate cells, such as dendritic cells, eosinophils, and natural killer (NK) cells (data not shown). Although DMOG treatment has been reported to affect the biology of neutrophils (Ong et al., 2018), we observed no changes in these cells in terms of mitochondrial potential and mROS production, despite the slight decrease in their total numbers in the lung of Mtb-infected mice treated with DMOG (data not shown), arguing for a direct effect on the macrophage compartment.

Recently, the regulation of glycolytic shift in metabolism by Akt-mTOR/HIF-1α signaling was elucidated with respect to trained immunity in macrophages (Cheng et al., 2014). Thus, impairment of the mTOR/HIF-1α axis by the TB-associated microenvironment may have important clinical implications leading to the long-term modulation of the innate immunity. This knowledge may contribute to future TB vaccine development by combining both innate and adaptive arms of the immune memory.

In conclusion, together with our previous work, this study contributes to the establishment of the acellular fraction of TB-PE as a physiologically relevant tuberculous milieu, demonstrating its capacity to shift macrophage metabolism to the advantage of the pathogen. Indeed, we propose that human macrophages committed to a pro-inflammatory profile to control infection can be metabolically reprogrammed by host-derived lipids generated during Mtb infection. Reprogrammed macrophages exhibited an OXPHOS metabolic program along with attenuated pro-inflammatory and microbicide properties, resulting in susceptibility to Mtb intracellular growth. It remains to be elucidated whether this metabolic shift also benefits the host as a disease-tolerance mechanism to avoid tissue damage, yet we are certain its use will be complementary to current models of TB investigation, providing a better understanding of the complex interaction between the host immune response and the bacilli and the tissue environment where it takes place.

STAR★METHODS

Detailed methods are provided in the online version of this paper and include the following:

- KEY RESOURCES TABLE
- RESOURCE AVAILABILITY
  - Lead Contact
  - Materials Availability
  - Data and Code Availability
- EXPERIMENTAL MODEL AND SUBJECT DETAILS
  - Human Subjects
  - Animal Studies
- METHOD DETAILS
  - Bacterial strain and antigens
  - Preparation of PE Pools
  - Preparation of Human Monocyte-Derived Macrophages
  - Macrophages treatments
  - Cell viability in macrophages
  - Determination of metabolites
  - Determination of glucose uptake
  - Measurement of cell respiration with Seahorse flux analyzer
  - Measurement of cell respiration with Oroboros
  - Phenotypic characterization by flow cytometry
  - Quantitative RT-PCR
  - Fluorescence microscopy
  - Transmission electron microscopy
  - Changes of mitochondrial membrane potential
  - Reactive oxygen species measurements
  - Soluble IL-1β determinations
  - Western blots
  - Infection of human macrophages with Mtb
  - Measurement of bacterial intracellular growth in macrophages by CFU assay
  - Visualization and quantification of Mtb infection
  - Mtb H37Rv infection and treatment with DMOG of mice
  - Immunofluorescence Microscopy
  - Proteins digestion of TB-PE
  - Total lipid and polar metabolite extractions
  - Lipidomic analysis of mycobacterial lipids
  - Lipidomic analysis of eicosanoids
- QUANTIFICATION AND STATISTICAL ANALYSIS

SUPPLEMENTAL INFORMATION

Supplemental Information can be found online at https://doi.org/10.1016/j.celrep.2020.108547.

ACKNOWLEDGMENTS

We thank the TRI-IPBS platform (Emmanuelle Naser and Antonio Peixoto) for flow cytometry and image analyses, the ANEXPLO-IPBS platform (Flavie Moreau and Céline Berrone) for maintenance of the ASB3 facility and the BSL3 multi-pathogen facility, and the MetaToul Lipidomic Core Facility (I2MC, INSERM 1048, Toulouse, France, MetaboHUB-ANR-11-INSB-0010) for assistance and access to the mass spectrometry instrument. We also thank Drs. Alexia Dumas and Yanick Poquet for providing the Mtb-mCherry strain, as well as Dr. Fabiana Bigi for providing the RFP-Mtb strain. In addition, we are grateful for the editing service provided by Life Science editors.

This work was supported by the Argentinean National Agency of Promotion of Science and Technology (PICT-2015-0055 to M.D.C.S. and PICT-2017-1317 to L.B.); the Argentinean National Council of Scientific and Technical Investigations (CONICET, PIP 112-2013-0100202 to M.C.S.); CONACYT/CONICET, the National Council of Science and Technology Mexico (CONACyT FC 2015-1/115 to M.C.S. and C.S.T.); the Centre National de la Recherche Scientifique; the Université Toulouse - III Paul Sabatier; the Agence Nationale de la Recherche (ANR-18-CE15-0004-01 to D.H.); Fondation pour la Recherche Medicale (ING20160435108 to E.L.); and the Agence Nationale de Recherche sur le Sida et les Hépatites Virales (ANRS2014-CI-2 and ANRS2014-049 to O.N. and ANRS 2020-1 to C.V. and G.L.-V.). The funders had no role in study design, data collection, analysis, decision to publish, or preparation of the manuscript.

AUTHOR CONTRIBUTIONS

Conceptualization and Methodology, J.L.M.F., D.C., A.M., J.P.-C., E.L., Y.R., D.C., D.H., G.L.-V., and L.B. Investigation, J.L.M.F., M.G., D.C., A.C., A.M., G.D., M.F., M.M., M.B.D., O.E.A.-T., E.P.-M., E.L., G.L.-V., and L.B. Resources, E.J.M., D.P., M.O., P.S., C.S.-T., R.H.-P., J.P.-C., D.H., O.N., C.V., I.M.P., M.D.C.S., and L.B. Writing, D.P., M.O., J.P.-C., D.H., O.N., C.V., D.C., E.L., G.L.-V., M.D.C.S., and L.B. Visualization, V.S., C.V., A.M., and F.F. Funding Acquisition, D.H., O.N., I.M.-P., C.V., G.L.-V., M.D.C.S., and L.B. L.B. and G.C. are responsible for ownership and responsibility that are inherent to aspects of this study.

DECLARATION OF INTERESTS

The authors declare no competing interests.

Received: February 28, 2020
Revised: October 18, 2020
Accepted: December 2, 2020
Published: December 29, 2020

REFERENCES

Abuaita, B.H., Schultz, T.L., and O'Riordan, M.X. (2018). Mitochondria-derived vesicles deliver antimicrobial reactive oxygen species to control phagosome-localized Staphylococcus aureus. Cell Host Microbe *24*, 625–636.e5.

Arnett, E., Weaver, A.M., Woodyard, K.C., Montoya, M.J., Li, M., Hoang, K.V., Hayhurst, A., Azad, A.K., and Schlesinger, L.S. (2018). PPARγ is critical for Mycobacterium tuberculosis induction of Mcl-1 and limitation of human macrophage apoptosis. PLoS Pathog. *14*, e1007100.

Baay-Guzman, G.J., Duran-Padilla, M.A., Rangel-Santiago, J., Tirado-Rodriguez, B., Antonio-Andres, G., Barrios-Payan, J., Mata-Espinosa, D., Klunder-Klunder, M., Vega, M.I., Hernandez-Pando, R., and Huerta-Yepez, S. (2018). Dual role of hypoxia-inducible factor 1 α in experimental pulmonary tuberculosis: its implication as a new therapeutic target. Future Microbiol. *13*, 785–798.

Bafica, A., Scanga, C.A., Serhan, C., Machado, F., White, S., Sher, A., and Aliberti, J. (2005). Host control of Mycobacterium tuberculosis is regulated by 5-lipoxygenase-dependent lipoxin production. J. Clin. Invest. *115*, 1601–1606.

Barham, D., and Trinder, P. (1972). An improved colour reagent for the determination of blood glucose by the oxidase system. Analyst (Lond.) *97*, 142–145.

Bhatt, K., and Salgame, P. (2007). Host innate immune response to Mycobacterium tuberculosis. J. Clin. Immunol. *27*, 347–362.

Boscá, L., González-Ramos, S., Prieto, P., Fernández-Velasco, M., Mojena, M., Martín-Sanz, P., and Alemany, S. (2015). Metabolic signatures linked to macrophage polarization: from glucose metabolism to oxidative phosphorylation. Biochem. Soc. Trans. *43*, 740–744.

Braverman, J., Sogi, K.M., Benjamin, D., Nomura, D.K., and Stanley, S.A. (2016). HIF-1α Is An Essential Mediator of IFN-γ-dependent immunity to *Mycobacterium tuberculosis*. J. Immunol. *197*, 1287–1297.

Cai, Y., Sugimoto, C., Liu, D.X., Midkiff, C.C., Alvarez, X., Lackner, A.A., Kim, W.-K., Didier, E.S., and Kuroda, M.J. (2015). Increased monocyte turnover is associated with interstitial macrophage accumulation and pulmonary tissue damage in SIV-infected rhesus macaques. J. Leukoc. Biol. *97*, 1147–1153.

Chen, M., Divangahi, M., Gan, H., Shin, D.S.J., Hong, S., Lee, D.M., Serhan, C.N., Behar, S.M., and Remold, H.G. (2008). Lipid mediators in innate immunity against tuberculosis: opposing roles of PGE 2 and LXA 4 in the induction of macrophage death. J. Exp. Med. *97*, 1147–1153.

Cheng, S.C., Quintin, J., Cramer, R.A., Shepardson, K.M., Saeed, S., Kumar, V., Giamarellos-Bourboulis, E.J., Martens, J.H.A., Rao, N.A., Aghajanirefah, A., et al. (2014). MTOR- and HIF-1α-mediated aerobic glycolysis as metabolic basis for trained immunity. Science *345*, 1250684.

Chinta, K.C., Rahman, M.A., Saini, V., Glasgow, J.N., Reddy, V.P., Lever, J.M., Nhamoyebonde, S., Leslie, A., Wells, R.M., Traylor, A., et al. (2018). Microanatomic distribution of myeloid heme oxygenase-1 protects against free radical-mediated immunopathology in human tuberculosis. Cell Rep. *97*, 1147–1153.

Cogliati, S., Enriquez, J.A., and Scorrano, L. (2016). Mitochondrial cristae: where beauty meets functionality. Trends Biochem. Sci. *41*, 261–273.

Cohen, S.B., Gern, B.H., Delahaye, J.L., Adams, K.N., Plumlee, C.R., Winkler, J.K., Sherman, D.R., Gerner, M.Y., and Urdahl, K.B. (2018). Alveolar macrophages provide an early Mycobacterium tuberculosis niche and initiate dissemination. Cell Host Microbe *24*, 439–446.e4.

Dennis, E.A., and Norris, P.C. (2015). Eicosanoid storm in infection and inflammation. Nat. Rev. Immunol. *15*, 511–523.

el-Ahmady, O., Mansour, M., Zoeir, H., and Mansour, O. (1997). Elevated concentrations of interleukins and leukotriene in response to Mycobacterium tuberculosis infection. Ann. Clin. Biochem. *34*, 160–164.

Finlay, D.K., Rosenzweig, E., Sinclair, L.V., Feijoo-Carnero, C., Hukelmann, J.L., Rolf, J., Panteleyev, A.A., Okkenhaug, K., and Cantrell, D.A. (2012). PDK1 regulation of mTOR and hypoxia-inducible factor 1 integrate metabolism and migration of CD8+ T cells. J. Exp. Med. *209*, 2441–2453.

Fischer, B., von Knethen, A., and Brüne, B. (2002). Dualism of oxidized lipoproteins in provoking and attenuating the oxidative burst in macrophages: role of peroxisome proliferator-activated receptor-γ. J. Immunol. *168*, 2828–2834.

Ganbat, D., Seehase, S., Richter, E., Vollmer, E., Reiling, N., Fellenberg, K., Gaede, K.I., Kugler, C., and Goldmann, T. (2016). Mycobacteria infect different cell types in the human lung and cause species dependent cellular changes in infected cells. BMC Pulm. Med. *16*, 19.

Gao, Z., Li, Y., Wang, F., Huang, T., Fan, K., Zhang, Y., Zhong, J., Cao, Q., Chao, T., Jia, J., et al. (2017). Mitochondrial dynamics controls anti-tumour innate immunity by regulating CHIP-IRF1 axis stability. Nat. Commun. *8*, 1805.

Genoula, M., Marín Franco, J.L., Dupont, M., Kviatcovsky, D., Milillo, A., Schierloh, P., Moraña, E.J., Poggi, S., Palmero, D., Mata-Espinosa, D., et al. (2018). Formation of foamy macrophages by tuberculous pleural effusions is triggered by the interleukin-10/signal transducer and activator of transcription 3 axis through ACAT upregulation. Front. Immunol. *9*, 459.

Genoula, M., Marín Franco, J.L., Maio, M., Dolotowicz, B., Ferreyra, M., Milillo, M.A., Mascarau, R., Moraña, E.J., Palmero, D., Matteo, M., et al. (2020). Fatty acid oxidation of alternatively activated macrophages prevents foam cell formation, but Mycobacterium tuberculosis counteracts this process via HIF-1α activation. PLoS Pathog. *16*, e1008929.

Gleeson, L.E., and Sheedy, F.J. (2016). Metabolic reprogramming & inflammation: fuelling the host response to pathogens. Semin. Immunol. *28*, 450–468.

Goletti, D., Petruccioli, E., Joosten, S.A., and Ottenhoff, T.H.M. (2016). Tuberculosis biomarkers: from diagnosis to protection. Infect. Dis. Rep. *8*, 6568.

Hackett, E.E., Charles-Messance, H., O'Leary, S.M., Gleeson, L.E., Muñoz-Wolf, N., Case, S., Wedderburn, A., Johnston, D.G.W., Williams, M.A., Smyth, A., et al. (2020). Mycobacterium tuberculosis limits host glycolysis and IL-1β by restriction of PFK-M via microRNA-21. Cell Rep. *30*, 124–136.e4.

Herb, F., Thye, T., Niemann, S., Browne, E.N.L., Chinbuah, M.A., Gyapong, J., Osei, I., Owusu-Dabo, E., Werz, O., Rüsch-Gerdes, S., et al. (2008). ALOX5 variants associated with susceptibility to human pulmonary tuberculosis. Hum. Mol. Genet. *17*, 1052–1060.

Huang, L., and Russell, D.G. (2017). Protective immunity against tuberculosis: what does it look like and how do we find it? Curr. Opin. Immunol. *48*, 44–50.

Huang, S.C.C., Smith, A.M., Everts, B., Colonna, M., Pearce, E.L., Schilling, J.D., and Pearce, E.J. (2016). Metabolic reprogramming mediated by the mTORC2-IRF4 signaling axis is essential for macrophage alternative activation. Immunity. *45*, 817–830.

Huang, L., Nazarova, E.V., Tan, S., Liu, Y., and Russell, D.G. (2018). Growth of *Mycobacterium tuberculosis* in vivo segregates with host macrophage metabolism and ontogeny. J. Exp. Med. *215*, 1135–1152.

Ip, W.K.E., Hoshi, N., Shouval, D.S., Snapper, S., and Medzhitov, R. (2017). Anti-inflammatory effect of IL-10 mediated by metabolic reprogramming of macrophages. Science *356*, 513–519.

Jaakkola, P., Mole, D.R., Tian, Y.M., Wilson, M.I., Gielbert, J., Gaskell, S.J., von Kriegsheim, A., Hebestreit, H.F., Mukherji, M., Schofield, C.J., et al. (2001). Targeting of HIF-α to the von Hippel-Lindau ubiquitylation complex by O2-regulated prolyl hydroxylation. Science *292*, 468–472.

Jaguin, M., Houlbert, N., Fardel, O., and Lecureur, V. (2013). Polarization profiles of human M-CSF-generated macrophages and comparison of M1-markers in classically activated macrophages from GM-CSF and M-CSF origin. Cell. Immunol. *281*, 51–61.

Juffermans, N.P., Florquin, S., Camoglio, L., Verbon, A., Kolk, A.H., Speelman, P., van Deventer, S.J.H., and van der Poll, T. (2000). Interleukin-1 signaling is essential for host defense during murine pulmonary tuberculosis. J. Infect. Dis. *182*, 902–908.

Kahnert, A., Seiler, P., Stein, M., Bandermann, S., Hahnke, K., Mollenkopf, H., and Kaufmann, S.H.E. (2006). Alternative activation deprives macrophages of a coordinated defense program to Mycobacterium tuberculosis. Eur. J. Immunol. *36*, 631–647.

Kelly, B., and O'Neill, L.A.J. (2015). Metabolic reprogramming in macrophages and dendritic cells in innate immunity. Cell Res. *25*, 771–784.

Kinet, S., Swainson, L., Lavanya, M., Mongellaz, C., Montel-Hagen, A., Craveiro, M., Manel, N., Battini, J.L., Sitbon, M., and Taylor, N. (2007). Isolated receptor binding domains of HTLV-1 and HTLV-2 envelopes bind Glut-1 on activated CD4+ and CD8+ T cells. Retrovirology *4*, 31.

Koo, M.S., Subbian, S., and Kaplan, G. (2012). Strain specific transcriptional response in Mycobacterium tuberculosis infected macrophages. Cell Commun. Signal. *10*, 2.

Lastrucci, C., Bénard, A., Balboa, L., Pingris, K., Souriant, S., Poincloux, R., Al Saati, T., Rasolofo, V., González-Montaner, P., Inwentarz, S., et al. (2015). Tuberculosis is associated with expansion of a motile, permissive and immunomodulatory CD16(+) monocyte population via the IL-10/STAT3 axis. Cell Res. *25*, 1333–1351.

Layre, E., Sweet, L., Hong, S., Madigan, C.A., Desjardins, D., Young, D.C., Cheng, T.Y., Annand, J.W., Kim, K., Shamputa, I.C., et al. (2011). A comparative lipidomics platform for chemotaxonomic analysis of Mycobacterium tuberculosis. Chem. Biol. *18*, 1537–1549.

Le Faouder, P., Baillif, V., Spreadbury, I., Motta, J.P., Rousset, P., Chêne, G., Guigné, C., Tercé, F., Vanner, S., Vergnolle, N., et al. (2013). LC-MS/MS method for rapid and concomitant quantification of pro-inflammatory and pro-resolving polyunsaturated fatty acid metabolites. J. Chromatogr. B Anal. Technol. Biomed. Life Sci. *932*, 123–133.

Light, R.W. (2010). Update on tuberculous pleural effusion. Respirology, 20345583.

Maertzdorf, J., Tönnies, M., Lozza, L., Schommer-Leitner, S., Mollenkopf, H., Bauer, T.T., and Kaufmann, S.H.E. (2018). Mycobacterium tuberculosis invasion of the human lung: first contact. Front. Immunol. *9*, 1346.

Marakalala, M.J., Raju, R.M., Sharma, K., Zhang, Y.J., Eugenin, E.A., Prideaux, B., Daudelin, I.B., Chen, P.Y., Booty, M.G., Kim, J.H., et al. (2016). Inflammatory signaling in human tuberculosis granulomas is spatially organized. Nat. Med. *22*, 531–538.

Martinez, F.O., Helming, L., and Gordon, S. (2009). Alternative activation of macrophages: an immunologic functional perspective. Annu. Rev. Immunol. *27*, 451–483.

Matta, S.K., and Kumar, D. (2016). Hypoxia and classical activation limits Mycobacterium tuberculosis survival by Akt-dependent glycolytic shift in macrophages. Cell Death Discov. *2*, 16022.

Mehrotra, P., Jamwal, S.V., Saquib, N., Sinha, N., Siddiqui, Z., Manivel, V., Chatterjee, S., and Rao, K.V.S. (2014). Pathogenicity of Mycobacterium tuberculosis is expressed by regulating metabolic thresholds of the host macrophage. PLoS Pathog. *10*, e1004265.

Mills, C. (2012). M1 and M2 macrophages: oracles of health and disease. Crit. Rev. Immunol. *32*, 463–488.

Mills, C.D., Kincaid, K., Alt, J.M., Heilman, M.J., and Hill, A.M. (2000). M-1/M-2 macrophages and the Th1/Th2 paradigm. J. Immunol. *164*, 6166–6173.

Mishra, B.B., Lovewell, R.R., Olive, A.J., Zhang, G., Wang, W., Eugenin, E., Smith, C.M., Phuah, J.Y., Long, J.E., Dubuke, M.L., et al. (2017). Nitric oxide prevents a pathogen-permissive granulocytic inflammation during tuberculosis. Nat. Microbiol. *2*, 17072.

Movafagh, S., Crook, S., and Vo, K. (2015). Regulation of hypoxia-inducible factor-1a by reactive oxygen species: new developments in an old debate. J. Cell. Biochem. *116*, 696–703.

Na, Y.R., Gu, G.J., Jung, D., Kim, Y.W., Na, J., Woo, J.S., Cho, J.Y., Youn, H., and Seok, S.H. (2017). Correction: GM-CSF induces inflammatory macrophages by regulating glycolysis and lipid metabolism. J. Immunol. *198*, 3000.

Narendran, G., Kavitha, D., Karunaianantham, R., Gil-Santana, L., Almeida-Junior, J.L., Reddy, S.D., Kumar, M.M., Hemalatha, H., Jayanthi, N.N., Ravichandran, N., et al. (2016). Role of LTA4H polymorphism in tuberculosis-associated immune reconstitution inflammatory syndrome occurrence and clinical severity in patients infected with HIV. PLoS ONE *11*, e0163298.

Ong, C.W.M., Fox, K., Ettorre, A., Elkington, P.T., and Friedland, J.S. (2018). Hypoxia increases neutrophil-driven matrix destruction after exposure to Mycobacterium tuberculosis. Sci. Rep. *8*, 11475.

Pace, E., Profita, M., Melis, M., Bonanno, A., Paternò, A., Mody, C.H., Spatafora, M., Ferraro, M., Siena, L., Vignola, A.M., et al. (2004). LTB4 is present in exudative pleural effusions and contributes actively to neutrophil recruitment in the inflamed pleural space. Clin. Exp. Immunol. *135*, 519–527.

Palsson-McDermott, E.M., and O'Neill, L.A.J. (2013). The Warburg effect then and now: from cancer to inflammatory diseases. BioEssays *35*, 965–973.

Palsson-Mcdermott, E.M., Curtis, A.M., Goel, G., Lauterbach, M.A.R., Sheedy, F.J., Gleeson, L.E., Van Den Bosch, M.W.M., Quinn, S.R., Domingo-Fernandez, R., Johnson, D.G.W., et al. (2015). Pyruvate kinase M2 regulates hif-1α activity and il-1β induction and is a critical determinant of the Warburg effect in LPS-activated macrophages. Cell Metab. *21*, 65–80.

Pavan Kumar, N., Moideen, K., Nancy, A., Viswanathan, V., Shruthi, B.S., Shanmugam, S., Hissar, S., Kornfeld, H., and Babu, S. (2019). Plasma eicosanoid levels in tuberculosis and tuberculosis-diabetes co-morbidity are associated with lung pathology and bacterial burden. Front. Cell. Infect. Microbiol. *9*, 335.

Pisu, D., Huang, L., Grenier, J.K., and Russell, D.G. (2020). Dual RNA-seq of Mtb-infected macrophages in vivo reveals ontologically distinct host-pathogen interactions. Cell Rep. *30*, 335–350.e4.

Raju, B., Hoshino, Y., Belitskaya-Lévy, I., Dawson, R., Ress, S., Gold, J.A., Condos, R., Pine, R., Brown, S., Nolan, A., et al. (2008). Gene expression profiles of bronchoalveolar cells in pulmonary TB. Tuberculosis (Edinb.) *88*, 39–51.

Rambold, A.S., and Pearce, E.L. (2018). Mitochondrial dynamics at the interface of immune cell metabolism and function. Trends Immunol. *39*, 6–18.

Rito, T., Ferreira, J., Cavadas, B., Soares, P., Oliveira, O., Richards, M.B., Duarte, R., Pereira, L., and Correia-Neves, M. (2019). Association of leukotriene A4 hydrolase with tuberculosis susceptibility using genomic data in Portugal. Microorganisms *7*, E650.

Rius, J., Guma, M., Schachtrup, C., Akassoglou, K., Zinkernagel, A.S., Nizet, V., Johnson, R.S., Haddad, G.G., and Karin, M. (2008). NF-kappaB links innate immunity to the hypoxic response through transcriptional regulation of HIF-1α. Nature *453*, 807–811.

Russell, D.G., Cardona, P.-J., Kim, M.-J., Allain, S., and Altare, F. (2009). Foamy macrophages and the progression of the human tuberculosis granuloma. Nat. Immunol. *10*, 943–948.

Russell, D.G., VanderVen, B.C., Lee, W., Abramovitch, R.B., Kim, M.J., Homolka, S., Niemann, S., and Rohde, K.H. (2010). Mycobacterium tuberculosis wears what it eats. Cell Host Microbe *8*, 68–76.

Schnappinger, D., O'Brien, K.M., and Ehrt, S. (2015). Construction of conditional knockdown mutants in mycobacteria. Methods Mol. Biol. *1285*, 151–175.

Seibert, A.F., Haynes, J., Jr., Middleton, R., and Bass, J.B., Jr. (1991). Tuberculous pleural effusion. Twenty-year experience. Chest *99*, 883–886.

Semba, H., Takeda, N., Isagawa, T., Sugiura, Y., Honda, K., Wake, M., Miyazawa, H., Yamaguchi, Y., Miura, M., Jenkins, D.M.R., et al. (2016). HIF-1α-PDK1 axis-induced active glycolysis plays an essential role in macrophage migratory capacity. Nat. Commun. *7*, 11635.

Shi, L., Salamon, H., Eugenin, E.A., Pine, R., Cooper, A., and Gennaro, M.L. (2015). Infection with Mycobacterium tuberculosis induces the Warburg effect in mouse lungs. Sci. Rep. *5*, 18176.

Souriant, S., Balboa, L., Dupont, M., Pingris, K., Kviatcovsky, D., Cougoule, C., Lastrucci, C., Bah, A., Gasser, R., Poincloux, R., et al. (2018). Tuberculosis Exacerbates HIV-1 Infection through IL-10/STAT3-Dependent Tunneling Nanotube Formation in Macrophages. Cell Rep *26*, 3586–3599.

Srivastava, A., and Mannam, P. (2015). Warburg revisited: lessons for innate immunity and sepsis. Front. Physiol. *6*, 70.

Subbian, S., Tsenova, L., Kim, M.J., Wainwright, H.C., Visser, A., Bandyopadhyay, N., Bader, J.S., Karakousis, P.C., Murrmann, G.B., Bekker, L.G., et al. (2015). Lesion-specific immune response in granulomas of patients with pulmonary tuberculosis: a pilot study. PLoS ONE *10*, e0132249.

Tannahill, G.M., Curtis, A.M., Adamik, J., Palsson-McDermott, E.M., McGettrick, A.F., Goel, G., Frezza, C., Bernard, N.J., Kelly, B., Foley, N.H., et al. (2013). Succinate is an inflammatory signal that induces IL-1β through HIF-1α. Nature *496*, 238–242.

Tobin, D.M., Roca, F.J., Oh, S.F., McFarland, R., Vickery, T.W., Ray, J.P., Ko, D.C., Zou, Y., Bang, N.D., Chau, T.T.H., et al. (2012). Host genotype-specific therapies can optimize the inflammatory response to mycobacterial infections. Cell *148*, 434–446.

Tobin, D.M., Roca, F.J., Ray, J.P., Ko, D.C., and Ramakrishnan, L. (2013). An enzyme that inactivates the inflammatory mediator leukotriene B4 restricts mycobacterial infection. PLoS One. *8*, e67828.

Trinder, P. (1969). Determination of blood glucose using an oxidase-peroxidase system with a non-carcinogenic chromogen. J. Clin. Pathol. *22*, 158–161.

Van den Bossche, J., O'Neill, L.A., and Menon, D. (2017). Macrophage immunometabolism: where are we (going)? Trends Immunol. *38*, 395–406.

Vorster, M.J., Allwood, B.W., Diacon, A.H., and Koegelenberg, C.F.N. (2015). Tuberculous pleural effusions: advances and controversies. J. Thorac. Dis. *7*, 981–991.

Wang, D., Malo, D., and Hekimi, S. (2010). Elevated mitochondrial reactive oxygen species generation affects the immune response via hypoxia-inducible factor-1α in long-lived Mclk1 +/− mouse mutants. J. Immunol. *184*, 582–590.

Weinberg, S.E., Sena, L.A., and Chandel, N.S. (2015). Mitochondria in the regulation of innate and adaptive immunity. Immunity *42*, 406–417.

West, A.P., Brodsky, I.E., Rahner, C., Woo, D.K., Erdjument-Bromage, H., Tempst, P., Walsh, M.C., Choi, Y., Shadel, G.S., and Ghosh, S. (2011). TLR signalling augments macrophage bactericidal activity through mitochondrial ROS. Nature *472*, 476–480.

World Health Organization (2019). Global tuberculosis report 2019 (WHO/CDS/TB/2019.15) (WHO). https://www.who.int/publications/i/item/global-tuberculosis-report-2019.

STAR★METHODS

KEY RESOURCES TABLE

REAGENT or RESOURCE	SOURCE	IDENTIFIER
Antibodies		
Anti-human CD14	Biolegend	RRID: AB_893253
Anti-human Glut1	R&D Systems	Cat# FAB1418P
Anti-human HIF-1α	Biolegend	RRID: AB_2562422
Anti-human mTOR pS2448	BD Biosciences	Cat# 563489
Anti-mouse CD45.2	BD Biosciences	RRID: AB_2738374
Anti-mouse MERTK	Thermo Fisher Scientific	RRID: AB_2688137
Anti-mouse SIGLEC-F	BD Biosciences	RRID: AB_274042
Anti-mouse CD64	Thermo Fisher Scientific	RRID: AB_2735010
Anti-mouse CD11c	Biolegend	RRID: AB_49356
Anti-mouse CD11b	Biolegend	RRID: AB_11125575
Anti-mouse Ly6G	BD Biosciences	RRID: AB_10611860
Anti-human human CD274 (B7-H1, PD-L1)	BD PharMingen	Cat# 557924
Anti-human CD86	Biolegend	RRID: AB_2734431
Anti-human CD80	Biolegend	RRID: AB_314501
Anti-human HLA-DR	BD Biosciences	Cat# 555811
Anti-human nuclear factor-kappa B (NF-κB) p65 (c-20)	Santa Cruz Biotechnology	Cat# sc-372
Anti-human-β-actin	Thermo Fisher Scientific	Cat #AM4302
Goat anti-mouse m-IgGκ BP-HRP	Santa Cruz Biotechnology	Cat# sc-516102
mouse anti-rabbit IgG, HRP	Santa Cruz Biotechnology	Cat# sc-2357
Rat IgG2b, κ Isotype Ctrl Antibody	Biolegend	RRID: AB_389343
Bacterial and Virus Strains		
M. tuberculosis H37Rv	N/A	N/A
Red fluorescent protein (RFP) expressing *M. tuberculosis* CDC 1551	Gift from Dr. Fabiana Bigi	INTA, Argentina
Mtb-mCherry	Gift from Dr. Yanick Poquet	IPBS, France
Biological Samples		
Patients-derived pleural effusions	Hospital F. J Muñiz (Buenos Aires, Argentina)	N/A
Buffy coats from healthy donors	Centro Regional de Hemoterapia Garrahan (Buenos Aires, Argentina)	N/A
Chemicals, Peptides, and Recombinant Proteins		
Human GM-CSF	Peprotech	Cat# 300-03
Human IFN-γ	Peprotech	Cat# 300-02
$H2_{RBD}$-EGFP	Gift from Dr. Matias Ostrowski	INBIRS, Argentina
DMOG	Bertin Technologies	Cat# 71210
Z-VAD-FMK (ZVAD)	Sigma-Aldrich	Cat# V116
Recombinant human IL-1RA protein (aILR1)	Abcam	Cat# ab50081
N-Acetyl-L-cysteine (NAC)	Sigma-Aldrich	Cat# A9165
Critical Commercial Assays		
Lactate Kit	Wiener	Cat# 1999795
Glicemia Enzimática AA Kit	Wiener	Cat# 1009803
2-NBDG	Invitrogen	Cat# N13195
Perm2 solution	BD Biosciences	Cat# 340973

(*Continued on next page*)

Continued

REAGENT or RESOURCE	SOURCE	IDENTIFIER
MitoSOX Red	Thermo Fisher Scientific	Cat# M36008
DiOC6(3) (3,3′-Dihexyloxacarbocyanine Iodide)	Thermo Fisher Scientific	Cat# D273
Trizol reagent	Thermo Fisher Scientific	Cat# 15596026
MitoSpy Green FM	Biolegend	Cat# 424805
JC-1	Invitrogen	Cat# 11570776
MitoSOX Red Mitochondrial Superoxide Indicator	Invitrogen	Cat# M36008
ELISA MAX Deluxe Set Human IL-1β	Biolegend	Cat# 437004
LIVE/DEAD Fixable Aqua Dead Cell	Thermofisher Scientific	Cat# L34957
OASIS HLB 96-well plate	Waters	Cat# WAT058951
Experimental Models: Organisms/Strains		
C57BL/6 mice	Charles River Laboratories	027
Software and Algorithms		
ImageJ	ImageJ	https://imagej.nih.gov/ij/
Prism (v5)	GraphPad	https://www.graphpad.com:443/
Photoshop CS3	Adobe	https://www.adobe.com/
Illustrator CS3	Adobe	https://www.adobe.com/
FlowJo 7.6.5	TreeStar	https://www.flowjo.com/
FCS Express V3	DeNovo Software	https://www.denovosoftware.com/
Seahorse Wave	Agilent	https://www.agilent.com
CFX Maestro	Bio-Rad	https://www.bio-rad.com/
DatLab 4	Oroboros Instruments	https://wiki.oroboros.at/index.php/OROBOROS_INSTRUMENTS
R	R Project	https://www.r-project.org/
Rstudio	Rstudio	https://rstudio.com/

RESOURCE AVAILABILITY

Lead Contact

Further information and requests for reagents should be directed to and will be fulfilled by the Lead Contact, Geanncarlo Lugo-Villarino (lugo@ipbs.fr).

Materials Availability

This study did not generate new unique reagents.

Data and Code Availability

This study did not generate/analyze any datasets or codes.

EXPERIMENTAL MODEL AND SUBJECT DETAILS

Human Subjects

Buffy coats from healthy donors were prepared at Centro Regional de Hemoterapia Garrahan (Buenos Aires, Argentina) according to institutional guidelines (resolution number CEIANM-664/07). Informed consent was obtained from each donor before blood collection.

PE were obtained by therapeutic thoracentesis by physicians at the Hospital F. J Muñiz (Buenos Aires, Argentina). The diagnosis of TB pleurisy was based on a positive Ziehl–Nielsen stain or Lowestein–Jensen culture from PE and/or histopathology of pleural biopsy, and was further confirmed by an Mtb-induced IFN-γ response and an adenosine deaminase-positive test (Light, 2010). Exclusion criteria included a positive HIV test, and the presence of concurrent infectious diseases or non-infectious conditions (cancer, diabetes, or steroid therapy). None of the patients had multidrug-resistant TB. Particularly, we studied 41 patients with PE that were divided according their etiology (Table S1 summarizes their clinical data, including gender and age). First two groups had 12 or 10 patients with tuberculous PE labeled as pool 1 and 2 respectively; second group had 6 patients with malignant PE (PE-C)

including mesothelioma, lung carcinoma or metastatic PE; third group had 8 patients with parapneumonic PE (PE-PNI); and forth group had 5 patients with transudates secondary to heart failure (HF-PE).

The research was carried out in accordance with the Declaration of Helsinki (2013) of the World Medical Association and was approved by the Ethics Committees of the Hospital F. J Muñiz and the Academia Nacional de Medicina de Buenos Aires (protocol number: NIN-1671-12, renewed in 2018; and 12554/17/X, respectively). Written informed consent was obtained before sample collection.

Animal Studies

Six- to eight-week-old female mice C57BL/6 were purchased from Charles River Laboratories. The experiments with these animals were performed in animal facilities based on the legal requirements in France and by qualified personnel that guarantee and minimize potential discomfort for the animals.

The procedures, including animal studies, were strictly conducted according with French laws and regulations in compliance with the European community council directive 68/609/EEC guidelines and its implementation in France.

METHOD DETAILS

Bacterial strain and antigens

The Mtb laboratory strain, H37Rv, was grown at 37°C in Middlebrook 7H9 medium supplemented with 10% albumin-dextrose-catalase (both from Becton Dickinson, New Jersey, USA) and 0.05% Tween-80 (Sigma-Aldrich, St. Louis, MO, USA). The Mtb γ-irradiated H37Rv strain (NR-49098) and corresponding total lipid preparation (NR-14837) were provided by BEI Resources, USA.

For some experiments in the mice model, a reporter strain of Mtb was constructed by transformation of wild-type Mtb strain with a reporter plasmid constructed by multisite gateway recombination using the procedures detailed by Schnappinger et al. (2015). The construct contains a module of the orf encoding the mCherry under the control of a constitutive promoter (P1). When transformed in Mtb, the construct is stably integrated in single copy at the att site of the L5 mycobacteriophage.

Preparation of PE Pools

The PE were collected in heparin tubes and centrifuged at 300 g for 10 minutes at room temperature without brake. The cell-free supernatant was transferred into new plastic tubes, further centrifuged at 12,000 g for 10 minutes and aliquots were stored at −80°C. After having the diagnosis of the PE, pools were prepared by mixing same amounts of individual PE associated to a specific etiology. The pools were decomplemented at 56°C for 30 minutes and filtered by 0.22 μm in order to remove any remaining debris or residual bacteria.

Preparation of Human Monocyte-Derived Macrophages

Peripheral blood mononuclear cells were obtained by Ficoll gradient separation on Ficoll-Paque (GE Healthcare, Amersham, UK). Then, monocytes were purified by centrifugation on a discontinuous Percoll gradient (GE Healthcare) as previously described (Genoula et al., 2018). After that, monocytes were allowed to adhere to culture plates (Costar) for 1 h at 37°C in warm RPMI-1640 medium (ThermoFisher Scientific, Waltham, MA). The cells were then washed with warm phosphate buffered saline (PBS) twice. The final purity was checked by fluorescence-activated cell sorting analysis using an anti-CD14 monoclonal antibody (mAb) and was found to be > 90%. The medium was then supplemented to a final concentration of 10% fetal bovine serum (FBS, Sigma-Aldrich) and human recombinant Granulocyte-Macrophage Colony-Stimulating Factor (GM-CSF, Peprotech, New Jork, USA) at 50 ng/ml. Cells were allowed to differentiate for 5–7 days leading to M0 macrophages.

Macrophages treatments

Macrophages were polarized toward M1 profile with IFN-γ (10 ng/ml) plus LPS (10 ng/ml), and then exposed (or not) to 20% v/v of PE during 24 h to generate PE-M1 and M1 cells, respectively. Alternatively, macrophages were stimulated with IFN-γ plus either irradiated Mtb (equivalent to a multiplicity of infection (MOI) of 2:1) or viable Mtb (MOI 5:1), and exposed (or not) to 20% v/v of PE for 24 h.

Cell viability in macrophages

The binding of FITC-Annexin V and propidium iodide (PI) staining in macrophages were measured according to the manufacturer's instructions (Molecular Probes, Oregon, USA), and cells were immediately analyzed by flow cytometry. Cell viability was also ascertained by lactate dehydrogenase (LDH) secretion test with a kinetic UV method kit according to the manufacturer's instructions (Roche Diagnostics GmbH, Germany).

Determination of metabolites

Lactate production and glucose concentrations in the culture medium was measured using the spectrophotometric assays Lactate Kit and Glicemia Enzimática AA Kit both from Wiener (Argentina), which are based on the oxidation of lactate or glucose, respectively, and the subsequent production of hydrogen peroxide (Barham and Trinder, 1972; Trinder, 1969). In particular, the consumption of

glucose was determined by assessing the diminution of glucose levels in culture supernatants in comparison with RPMI 10% FBS. The absorbance was read using a Biochrom Asys UVM 340 Microplate Reader microplate reader and software.

Determination of glucose uptake

Macrophages were incubated with the fluorescent glucose analog 2-(N-(7-Nitrobenz-2-oxa-1,3-diazol-4-yl)Amino)-2-Deoxyglucose (2-NBDG) (10 μM, Invitrogen, California, USA) in PBS for 30 min. Thereafter, cells were washed and intracellular 2-NBDG was measured by flow cytometry.

Measurement of cell respiration with Seahorse flux analyzer

XFp Extracellular Flux Analyzer (Seahorse Bioscience) can measure the rate of mitochondrial oxidative phosphorylation, through determination of the real-time oxygen consumption rate (OCR) measured in picomoles/min, on a 96 microplate-based assay platform. For this methodology, basal respiration was calculated as the last measurement before addition of the electron transport chain inhibitor oligomycin (OM) at 3 μM minus the non-mitochondrial respiration, which is the minimum rate measurement after addition of electron transport chain inhibitors rotenone (ROT) and antimycin (AA) at 0.5 μM. Estimated ATP production designates the last measurement before addition of OM minus the minimum rate after OM. Maximal respiration rate (max) was defined as the OCR after addition of OM and FCCP. Spare respiration capacity (SRC) was defined as the difference between max and basal respiration. Following this approach, OCR was determined in macrophages ($1.6x10^5$ cells/well) in 3 wells for each condition. The assay was performed in XF Assay Modified DMEM. Three consecutive measurements were performed under basal conditions and after the sequential addition of the following electron transport chain inhibitors.

Measurement of cell respiration with Oroboros

Cells were harvested and centrifuged, and the cellular pellet was resuspended in RPMI-1640 medium to the desired cellular concentration (typically in a range of $0.8 – 1 \times 10^7$ cells/ml). Respiration rate of intact cells was measured at 37°C with Oroboros high resolution respirometer Oxygraph-2k (Oroboros Instruments GmbH, Austria). Oxygraph-2k possesses two separate 2-mL chambers equipped with polarographic oxygen sensors that can measure in real time both the oxygen concentration (nanomoles/milliliter) and the oxygen consumption (picomoles/second/milliliter) within each chamber. The basic principle of the system is to measure the concentration and consumption of oxygen by injecting substrates directly to cells that are suspended in solution within the chamber. In our case, routine respiration was obtained soon after succinate (10mM) addition to the system. Thereafter, OM (10mM) was added to inhibit OXPHOS respiration, allowing the measurement of the contribution of mitochondrial respiration leak. By using ROT (1mM) and AA (4mM), we determined the residual oxygen consumption, ROX, which is respiration due to oxidative side reactions remaining after inhibition of the electron transfer-pathway. These ROX determinations were used to correct the values of ORC associated to routine and leak. With these parameters, we then calculated OXPHOS activity as follows: OXPHOS = (Routine - ROX) – (Leak - ROX). To determine the activity of complex IV of the electron transfer-pathway, ascorbate (ASC, 5mM) and *N,N,N',N',* tetramethyl-*p*-phenylenediamine (TMPD, 5mM), artificial electron donors reducing cytochrome *c*, were added to obtain the maximal activity associated to complex IV, which was then inhibited by adding potassium cyanide (KCN, 25mM). The values of ORC before and after KCN were used to calculate the net activity of complex IV (CIV). Data was analyzed with DatLab 4 software (Oroboros Instruments, Austria).

Phenotypic characterization by flow cytometry

Macrophages were centrifuged for 7 min at 1200 rpm and then stained for 40 min at 4°C with fluorophore-conjugated antibodies FITC-anti-HLA-DR (clone G46-6, BD Biosciences), PerCP.Cy5.5-anti-CD86 (clone 374216, Biolegend), PE-anti-PD-L1 (clone MIH1, BD PharMingen), or PE-anti-CD80 (clone 2D10, Biolegend), and in parallel, with the corresponding isotype control antibody. Additionally, macrophages were stained for 40 minutes at 4°C with fluorophore-conjugated antibodies PE-anti-Glut1 (clone 202915 R&D Systems, Minnesota, USA) and in parallel, with the corresponding isotype control antibody. Glut1 expression was also confirmed by labeling the cells with the ligand for Glut1, $H2_{RBD}$-EGFP (Kinet et al., 2007). After staining, the cells were washed with PBS 1X, centrifuged and analyzed by flow cytometry using FACSCalibur cytometer (BD Biosciences, San Jose, CA, USA). For HIF-1α and mTOR determination, macrophages were permeabilized with either methanol for HIF-1α or Perm2 solution for mTOR (BD Biosciences), and incubated with PE-anti-HIF-1α (clone 546-16, Biolegend, San Diego, USA) or PE-anti-mTOR (pS2448, BD Biosciences), respectively. The macrophage population was gated according to its Forward and Size Scatter properties. The median fluorescence intensity (MFI) was analyzed using FCS Express V3 software (*De Novo* Software, Los Angeles, CA, USA). For mice experiments, cell surface staining of single-cell suspensions from lungs was performed using fluorophore-conjugated antibodies: CD45.2, MERTK (clone DS5MMER), SIGLEC-F (clone E50-2440), CD64 (clone 10.1), Ly6G (1A8), CD11c (clone N418), CD11b (clone M1/70) and Live/Dead (LIVE/DEAD Fixable Aqua Dead Cell, Thermofisher Scientific). For analysis of mitochondrial markers, cells were stained with MitoSOX Red (5 μM) and DiOC6 (40nM) (ThermoFisher) at 37°C for 30 min. Cell staining was analyzed using a FACSAria Fusion cytometer in BSL3 facility and FlowJo software version V10. Cells were first gated on singlets (FSC-H versus FSC-W and SSC-H versus SSC-W) and live cells before further analyses.

Quantitative RT-PCR

Total RNA was extracted with Trizol reagent (Thermo Fisher Scientific) and cDNA was reverse transcribed using the Moloney murine leukemia virus reverse transcriptase and random hexamer oligonucleotides for priming (Life Technologies, CA, USA). The expression of the genes of hexokinase 2 (HK2) and LDH-A was determined using PCR SYBR Green sequence detection system (Eurogentec, Seraing, Belgium) and the CFX Connect Real-Time PCR Detection System (Bio-Rad, CA, United States). Gene transcript numbers were standardized and adjusted relative to eukaryotic translation elongation factor 1 alpha 1 (EeF1A1) transcripts. Gene expression was quantified using the ΔΔCt method. Primers used for RT-PCR were as follows: EeF1A1 Fwd: 5′- CCAAGACCCAGGCAT ACTTGGA-3′ and Rev: 5′-TCGGGCAAGTCCACCACTAC-3′; HK2 Fwd: 5′-GAGCCACCACTCACCCTACT-3′ and Rev: 5′-CCAGGC ATTCGGCAATGTG-3′; and LDH-A Fwd: 5′-TGGGAGTTCACCCATTAAGC-3′ and Rev: 5′-AGCACTCTCAACCACCTGCT-3′.

Fluorescence microscopy

Cells were stained with 250 nM MitoSpy Green FM (Biolegend) for 30 minutes. The cells were then washed with PBS three times. All the samples were imaged on a FluoView FV1000 confocal microscope (Olympus, Tokyo, Japan) equipped with a Plapon 60X/NA1.42 objective. To quantify the mitochondrial morphology of MitoSpy Green FM-stained macrophages, we developed a computer-aided analysis tool scoring the mitochondrial length and number per cell with ImageJ-Fiji software. Briefly, we used a motorized z-focus to obtain 3D images spanning the entire height of blindly selected cells to capture the entire architecture of the mitochondrial network and combined them into a single image using a maximum intensity projection. A threshold was defined to identify mitochondria based on their fluorescence intensity, and images were 'skeletonized' to measure mitochondrial length (perimeter) and number. At least 20 cells per condition were analyzed in each independent experiment.

Transmission electron microscopy

Macrophages were fixed in 2.5% glutaraldehyde/ 2% paraformaldehyde (EMS, Delta-Microscopies) dissolved in 0.1 M Sorensen buffer (pH 7.2) during 2h at room temperature, and then preserved in 1% paraformaldehyde (PFA) dissolved in Sorensen buffer. Adherent cells were treated for 1 h with 1% aqueous uranyl acetate then dehydrated in a graded ethanol series and embedded in Epon. Sections were cut on a Leica Ultracut microtome and ultrathin sections were mounted on 200 mesh onto Formvar carbon-coated copper grids. Finally, thin sections were stained with 1% uranyl acetate and lead citrate and examined with a transmission electron microscope (Jeol JEM-1400) at 80 kV. Images were acquired using a digital camera (Gatan Orius).

Changes of mitochondrial membrane potential

Mitochondrial membrane potential was measured using the mitochondrial-specific dual-fluorescence probe, 5,5′,6,6'-tetrachloro-1,1',3,3′-tetraethylbenzimidazolylcarbocyanine iodide (JC-1, Molecular Probes, Eugene, OR, USA). Macrophages were washed twice in ice-cold PBS and loaded with 2 μM JC-1 for 30 min, and then measured by flow cytometry (FACScan, BD Biosciences). In parallel, mitochondrial mass was determined in individual cells by labeling them with the probe MitoSpy Green FM (Biolegend). Green fluorescence was analyzed by flow cytometry.

Reactive oxygen species measurements

To measure the mROS superoxide, macrophages were incubated with MitoSOX (Molecular Probes) at 2.5 μM in serum-free RPMI media for 15 to 30 minutes at 37°C. Cells were washed with warmed PBS, removed from plates with cold PBS containing 1 mM ethylenediamine tetraacetic acid (EDTA) by pipeting, pelleted at 1500 rpm for 3 minutes, immediately resuspended in cold PBS containing 1% FBS, and subjected to FACS analysis.

Soluble IL-1β determinations

The amounts of human IL-1β were measured by ELISA, according to manufacturer's instructions kits (ELISA MAX Deluxe Kits from Biolegend). The detection limit was 15.6 pg/ml.

Western blots

Macrophages were lysed in ice-cold buffer consisting of 150 mM NaCl, 10 mM Tris, 5 mM EDTA, 1% Sodium Dodecyl Sulfate (SDS), 1% Triton X-100, 1% sodium deoxycholate, gentamicin/streptomycin, 0.2% azide plus a cocktail of protease inhibitors (Sigma-Aldrich). Lysates were incubated on ice for 3 h and cleared by centrifugation for 15 minutes at 14,000 rpm at 4°C. Protein concentrations were determined using the bicinchoninic acid (BCA) protein assay (Pierce, ThermoFisher). Equal amounts of protein (40 μg) were then resolved on a 10% SDS-PAGE. Proteins were transferred to Hybond-ECL nitrocellulose membranes (GE Healthcare) for 2 h at 100 V and blocked with 1% Bovine Serum Albumine (BSA)-0.05% Tween-20 for 1 h at room temperature. Membranes were probed with primary anti-human nuclear factor-kappa B (NF-κB) p65 (c-20) sc-372 (1:200 dilution, Santa Cruz Biotechnology, Palo Alto, CA, USA) overnight at 4°C. After extensive washing, blots were incubated with a horseradish peroxidase (HRP)-conjugated goat anti-rabbit IgG Ab (1:5000 dilution; Santa Cruz Biotechnology) for 1 h at room temperature. Immunoreactivity was detected using ECL Western Blotting Substrate (Pierce). Protein bands were visualized using Kodak Medical X-Ray General Purpose Film. For internal loading controls, membranes were stripped by incubating in buffer consisting of 1.5% Glycine, 0.1% SDS, 1% Tween-20, pH 2.2 for 10 minutes twice, extensively washed and reprobed with anti-β-actin (1:2000 dilution; ThermoFisher, clone AC-15) and or

HRP-conjugated goat anti-mouse IgG Ab (1:2000 dilution; Santa Cruz Biotechnology). Results from western blot were analyzed by densitometric analysis (ImageJ software).

Infection of human macrophages with Mtb

Infections were performed in the biosafety level 3 (BSL-3) laboratory at the *Unidad Operativa Centro de Contención Biológica (UOCCB), ANLIS-MALBRAN* (Buenos Aires), according to the biosafety institutional guidelines. Macrophages were infected with Mtb H37Rv strain at a MOI of 1-5:1 during 1 h at 37°C. Next, extracellular bacteria were removed gently by washing with pre-warmed PBS, and cells were cultured in RPMI-1640 medium supplemented with 10% FBS and gentamicin (50 μg/ml). Alternatively, macrophages were infected with the reference virulent or avirulent strains, H37Rv or H37Ra respectively, or with clinical isolates from the Latin American Mediterranean genotype (LAM9005186, considered a hypervirulent isolate), or the Beijing lineage (Bei 583, considered highly virulent), during 1 h at 37°C. Then, extracellular bacteria were removed gently by washing with pre-warmed PBS, and cells were cultured in RPMI-1640 medium supplemented with 10% FBS and gentamicin (50 μg/ml) for 4 and 24h. All strains were grown in Middlebrook 7H9 supplemented with 10% OADC. Strains were grown to logarithmic phase and measurement of the optical density determined the culture concentrations by spectrometry at 600 nm. Working aliquots were stored at −80°C until their use. Bacillary viability was tested by measuring the number of colonies forming units (CFU).

Measurement of bacterial intracellular growth in macrophages by CFU assay

When indicated, Z-VAD-FMK (ZVAD, 5μM) was added to macrophages or not 1 h prior to Mtb infection, then cells were rinsed two times with PBS 1x and RPMI-1640 medium supplemented with 10% FBS was renewed. Macrophages stimulated or not with IFN-γ were infected with Mtb H37Rv strain at a MOI of 0.5 bacteria/cell in the presence (or not) of TB-PE (triplicates). Alternatively, macrophages were treated with either *N*-Acetyl-L-cysteine (NAC, 1mM) or the recombinant human IL-1RA protein (aIL1R, 200ng/ml) in the presence or not of DMOG during Mtb infection respectively. After 24 h, extracellular bacteria were removed by gently washing four times with pre-warmed PBS and cells were cultured in RPMI-1640 medium supplemented with 10% FBS and gentamicin (50 μg/ml). In the case of the cultures treated with aIL1R and NAC, the drugs were renewed in fresh complete media after cell-washing. At different time points, cells were lysed in 0.1% SDS and neutralized with 20% BSA in Middlebrook 7H9 broth. Serial dilutions of the lysates were plated in triplicate, onto 7H11-Oleic Albumin Dextrose Catalase (OADC, Becton Dickinson) agar medium for CFU scoring at 21 days later.

Visualization and quantification of Mtb infection

Macrophages seeded on glass coverslips within a 24-well tissue culture plate at a density of 5×10^5 cells/ml were infected with the red fluorescent protein (RFP) expressing Mtb CDC 1551 strain at a MOI of 5:1 during 2 h at 37°C. Then, extracellular bacteria were removed gently by washing with pre-warmed PBS, and cells were cultured in RPMI-1640 medium supplemented with 10% FBS for 48 h. The glass coverslips were fixed with PFA 4% and stained with BODIPY 493/503 (Life Technologies). Finally, slides were mounted and visualized with a FluoView FV1000 confocal microscope (Olympus, Tokyo, Japan) equipped with a Plapon 60X/NA1.42 objective, and analyzed with the software ImageJ-Fiji. We measured the occupied area with RFP-Mtb (expressed as Raw Integrated Density) per cell in z stacks from confocal laser scanning microscopy images. Individual cells were defined by boron-dipyrromethene (BODIPY)-stained cellular membranes, which allow us to define the region of interests for quantification. For quantification 80-100 cells of random fields per condition were analyzed.

Mtb H37Rv infection and treatment with DMOG of mice

Experimental mice were anesthetized with a cocktail of ketamine (60 mg/kg, Merial) and xylasine (10 mg/kg, Bayer) and infected intranasally with ≈1000 CFUs of the Mtb experimental strain, H37Rv, in 25 μL of PBS. For drug treatment, mice received 1.25 mg of DMOG (Bertin Technologies) intraperitoneally per mouse every day starting upon infection for 14 days.

After the mice were sacrificed, the lungs were harvested aseptically, homogenized using a gentle MACS dissociator (C Tubes, Miltenyi, Biotec, CA, USA), and incubated with DNase I (0.1 mg/mL, Roche) and collagenase D (2 mg/mL, Roche) during 30 minutes at 37°C under 5% CO_2. The Mtb load was determined by plating serial dilutions of the lung homogenates onto 7H11 solid medium supplemented with OADC (Middlebrook). The plates were incubated at 37°C for 3 weeks before bacterial CFUs scoring. Lungs homogenates were filtered on 40 μm cell strainers and centrifuged at 329 × *g* during 5 min. Red blood cells were lysed in 150 mM NH_4Cl, 10 mM $KHCO_3$, 0.1 mM EDTA (pH 7.2).

Immunofluorescence Microscopy

Experimental mice were infected intranasally with ≈1000 CFUs of the H37Rv Mtb expressing mCherry, and were treated (or not) with DMOG every day starting upon infection for 14 days. Prior to euthanasia, 2ug of BV421-conjugated anti-SIGLEC-F were administrated intranasally 30 min before sacrifice before sacrifice. Mice were euthanized by intraperitoneal administration of pentobarbital (Doléthal, Vétoquinol, Lure, France) at lethal dose. Lung were fixed for 22 h at 4°C in PLP (0.075 M lysine, 0.37 M sodium phosphate pH 7.2, 2% formaldehyde, and 0.01 M NaIO4), washed twice in PBS and dehydrated in 30% sucrose for at least 24 h at 4°C prior to embedding in OCT and snap-frozen in isopentane pre-cooled by liquid nitrogen. 10 μm frozen sections (Leica CM1950) were stained with CD11b AF647 (M1/70, Biolegend 10122, 1:100) overnight at 4°C and adhered to a coverslip with Fluorescence Mounting

Medium (DAKO S3023). Images (Siglec-F BV421, Mtb-cherry, CD11b AF647) were acquired using a Zeiss Axio Imager M2 using a X10/0.3 EC Plan Apochromat or a X40/0.95 Plan Apochromat objective (Zeiss). Images were acquired and processed using the Zeiss Zen software and ORCA-flash 4.0 LT (Hamamatsu) camera.

Proteins digestion of TB-PE

Proteinase K (50 ug/mL, Sigma Aldrich) was immobilized by entrapment in polyacrylamide gel, and pieces of it were incubated with TB-PE overnight at 37°C to generate Pk PE. As control TB-PE was treated with polyacrilamide alone (Mock PE). Pk PE and Mock PE were centrifuged at high speed and the supernatant was collected and stored at −80°C until used. Protein digestion was controlled using sodium dodecyl sulfate polyacrylamide gel electrophoresis (SDS-PAGE), followed by Commassie blue staining.

Total lipid and polar metabolite extractions

Polar metabolites (PMPE) and lipids (LPE) extractions from TB-PE were based on Bligh and Dyer protocol. Briefly, 1 mL of TB-PE was transferred to 5 mL glass tubes containing 1.5 mL $CHCl_3$/CH_3OH (2:1, v/v). The samples were incubated overnight at 4°C with gentle agitation. After centrifugation, top layers were subjected to an additional extraction using $CHCl_3$:CH_3OH (1:2, v/v) and centrifuging at high speed for 2 minutes. The upper aqueous and organic lower phases, primarily PMPE and LPE, respectively, were collected and dried under vacuum. PMPE were resuspended in 12.5 μL of water, while LPE in 12.5 μL of DMSO. PMPE and LPE fractions were used at the same concentration as in the untouched TB-PE (1x) or at a double dose (2x). When indicated, eicosanoids were extracted from PE pools by a solid phase extraction method using Oasis HLB96-well clusters, as previously described (Le Faouder et al., 2013).

Lipidomic analysis of mycobacterial lipids

For the screening of the *M. tuberculosis* lipid families, TB-PE lipid extracts were resuspended at 0.5 mg/mL in $CHCl_3$/CH_3OH (1:1, v/v) and analyzed using a Waters Xevo G2-XS Q-Tof mass spectrometer coupled to a Waters Supercritical Fluid Chromatography ACQUITY UPC2 at the MetaToul Lipidomic Core Facility (I2MC, Inserm 1048, Toulouse, France). One microliter of lipid extract was injected on a Waters Torus DIOL column (1.7 μm x 100 mm x 3 mm) and the lipid families were separated using a gradient of CH_3OH (1%–50%) in CO_2, which allows the detection of Mtb lipids families with characteristic retention time, acylform profiles and accurate m/z, as previously described (Layre et al., 2011). Spectra were collected in positive and negative-ion mode from m/z 100 to 3000. Characteristic signals of phthiocerol dimycocerosate, glucose/trehalose monomycolate, sulfoglycolipids, tuberculosinyl adenosines, triglycosylated phenolic glycolipids or phosphatidyl-*myo*-inositol mannosides, could not be extracted from the dataset obtained for LPE samples (within 10 ppm accuracy).

Lipidomic analysis of eicosanoids

The analyze of eicosanoids was performed according to previous reports (Le Faouder et al., 2013). Briefly, 300 μL of cold methanol and 5 μL of internal standard (Deuterium labeled compounds) were added to 250 μL of PE samples. After centrifugation at 2000 g for 15 min at 4°C, supernatants were transferred into 2 mL 96-well deep plates and diluted in H_2O to 2 mL. Samples were then submitted to solid phase extraction (SPE) using OASIS HLB 96-well plate (30 mg/well, Waters) pretreated with MeOH (1 mL) and equilibrated with 10% MeOH (1 mL). After sample application, extraction plate was washed with 10% MeOH (1 mL). After drying under aspiration, lipids mediators were eluted with 1 mL of MeOH. Prior to LC-MS/MS analysis, samples were evaporated under nitrogen gas and reconstituted in 10 μL on MeOH. LC-MS/MS analyses of eicosanoids were performed as described (below reference). Briefly, lipid mediators were separated on a ZorBAX SB-C18 column (2.1 mm, 50 mm, 1.8 μm) (Agilent Technologies) using Agilent 1290 Infinity HPLC system (Technologies) coupled to an ESI-triple quadruple G6460 mass spectrometer (Agilent Technologies). Data were acquired in Multiple Reaction Monitoring (MRM) mode with optimized conditions (ion optics and collision energy). Peak detection, integration and quantitative analysis were done using Mass Hunter Quantitative analysis software (Agilent Technologies) based on calibration lines built with commercially available eicosanoids standards (Cayman Chemicals).

QUANTIFICATION AND STATISTICAL ANALYSIS

All values are presented as mean and standard error of the mean SEM of a number of independent experiments. Independent experiments are defined as those performed with macrophages derived from monocytes isolated independently from different donors. As most of our datasets did not pass the normality tests, non-parametric tests were applied. Comparisons between more than two paired datasets were made using the Friedman test followed by Dunn's Multiple Comparison Test. Comparisons between two paired experimental conditions were made using the two-tailed Wilcoxon Signed Rank. For the analysis of the OCR measurements, t test was applied. Comparisons between control or DMOG-treated mice were performed using the Mann-Whitney test. Multivariate analysis of lipidomics' data were performed by principal component analysis with the FactoMineR package in R software. For all statistical comparisons, a p value < 0.05 was considered significant.